Diagrammatic Design of Ansätze for Quantum Chemistry

Ayman El Amrani

St. John's College

A thesis submitted for the Honour School of Chemistry

Part II 2024

Pour ma mère et mon père.

Summary

A central challenge in computational quantum chemistry is the accurate simulation of fermionic systems. At the heart of these calculations lies the need to solve the Schrödinger equation to determine the many-electron wavefunction. Since an exact solution to this problem scales exponentially with the number of electrons, and classical computers have no means by which to efficiently store the increasingly large wavefunctions, this problem becomes computationally intractable for large and strongly-correlated systems [1]. In contrast, gate-based quantum computing presents a promising solution, offering the potential to represent electronic wavefunctions with polynomially scaling resources using quantum algorithms for the simulation of chemical systems [2]. In other words, quantum computers are a natural tool of choice for simulating processes that are inherently quantum [3].

In the last two decades, many advancements in quantum computing have been made in both hardware and software, bringing us closer to being able to simulate molecular systems. Despite these advancements, we remain in the so-called Noisy Intermediate Scale Quantum (NISQ) era [4], characterised by challenges such as poor qubit fidelity, low qubit connectivity and limited coherence times. The NISQ era represents a transitional phase in quantum computing, where quantum devices are not yet error-corrected but are still capable of performing computations beyond the reach of classical computers. Overcoming the limitations of the NISQ era is crucial for realising the full potential of quantum computing in various fields, including quantum chemistry and materials science.

In this thesis, we focus on the Unitary Product State (UPS) ansatz [5], implemented

on quantum devices using the Variational Quantum Eigensolver (VQE) algorithm [6]. In particular, we are concerned with the study of the excitation operators used to prepare UPS ansätze representing fermionic wavefunctions. The VQE algorithm is a method used to estimate the ground state energy of a molecular Hamiltonian by preparing a trial wavefunction, calculating its energy expectation value on a quantum device, then optimising the wavefunction parameters classically until the energy converges to the best approximation for the ground state energy [7]. It is recognised as a leading algorithm for quantum simulation on NISQ devices due to its reduced resource requirements in terms of qubit count and coherence time [8].

We build on the work of Yeung [3] on Pauli gadgets, Yordanov *et al* [9] on fermionic excitation operators and Cowtwan *et al* [10], concerning ourselves with two main questions: can we use the ZX calculus to gain insights into the structure of the UPS ansatz in the context of VQE algorithms for quantum chemistry? Secondly, in the context of NISQ devices, can we use these insights to build better ansätze with reduced circuit depth and more efficient resources? By attempting to reduce circuit depth, we are addressing the major source of error present in NISQ devices – the noise of today's quantum hardware [10].

- **Chapter 1** develops the mathematical foundation for simulating molecules on quantum computers.
- **Chapter 2** introduces the generators of the ZX calculus and its rewrite rules.
- **Chapter 3** introduces Pauli gadgets, the basic building blocks of fermionic ansätze, and their interaction with other quantum gates.
- **Chapter 4** explores controlled rotations in terms of phase polynomials.
- **Chapter 5** applies the theory developed thus far to show how excitation operators can be expressed it terms of controlled rotations in the ZX calculus.
- **Chapter 6** introduces the software package ZxFermion that we built, demonstrating how it can be used to replicate the research done in this thesis.

Contents

1 Background **1**

1.1 Context & Motivation 2

1.2 Electronic Structure Theory 4

1.3 Fundamentals of Quantum Computating 8

1.4 The Variational Quantum Eigensolver 12

2 ZX Calculus **15**

2.1 Generators 16

2.2 Rewrite Rules 20

2.3 Clifford Conjugation 23

3 Pauli Gadgets **24**

3.1 Phase Gadgets 25

3.2 Pauli Gadgets 28

3.3 Phase Polynomials 29

3.4 Commutation Relations 30

4 Controlled Rotations **35**

4.1 Singly Controlled-Rotations 36

4.2 Higher Order Controlled-Rotations 37

5 Excitation Operators **39**

5.1 Implementing Excitation Operators 40

5.2 Commuting Excitation Operators 44

5.3 Excitations as Controlled Rotations 45

6 ZxFermion Software **49**

6.1 Creating Gadgets and Circuits 50

6.2 Manipulating Circuits 52

7 Conclusion **55**

7.1 Summary 55

7.2 Future Work 55

Bibliography **56**

Chapter 1

Background

In this chapter, we begin by discussing the context and motivation for the research conducted in this thesis, then develop the theoretical foundation required to simulate fermionic systems on quantum computers. We start by giving an overview of Electronic Structure Theory in Section 1.2. We then introduce the Fundamentals of Quantum Computation in Section 1.3. Finally, we introduce the Variational Quantum Eigensolver (VQE) algorithm in Section 1.4.

1.1 Context & Motivation

Using the ZX calculus, this thesis focuses on the diagrammatic representation of excitation operators used to account for the correlation in fermionic systems. The ZX calculus is diagrammatic language for reasoning about quantum processes [11] that has recently shown an increased usage in quantum computing and quantum simulation. The research represented in this thesis is conducted within the framework of the *Variational Quantum Eigensolver (VQE)*, a promising hybrid quantum-classical algorithm for achieving quantum advantage on *Noise Intermediate-Scale Quantum (NISQ)* devices [12].

The VQE algorithm divides the problem of estimating the ground-state energy of a molecule into two parts: computing the energy of some fermionic state on a quantum device, then classically optimising the quantum circuit representing the state until it converges to a good approximation of the true ground state. The *Unitary-Product State (UPS)* ansatz, derived from the *Unitary Coupled Cluster (UCC)* formulation of the wavefunction, allows us to implement parametrised representations of fermionic states on a quantum computer.

The VQE algorithm generates multiple distinct UPS ansätze, each yielding the same energy expectation value. Hence, while different sequences of unitary excitation operators are employed to rotate the reference state to a state approximating the true ground state, their identical energy expectation values suggests that they equivalently capture the correlation present in the ground state, implying that that it may be possible to demonstrate the equivalence between these UPS ansätze through algebraic manipulation.

In this context, the research presented in this thesis focuses on the diagrammatic representation of unitary excitation operators in the ZX calculus. Our initial goal was to identify a generalised structure for these excitation operators within the ZX calculus, anticipating that by doing so, we might discover a way of demonstrating the equivalence of different VQE ansätze with the same energy expectation value. By developing a representation for these excitation operators that is independent

of specific architectural constraints, we sought to gain deeper insights into the structure of UPS ansätze and the nature of correlations in molecular quantum systems. This broader understanding could potentially lead to more efficient and effective quantum simulation algorithms. Furthermore, due to the poor fidelity of today's quantum computers, reducing the depth of quantum circuits is crucial to minimise errors in simulations. By identifying a generalised structure for the excitation operators used in the UPS ansatz, we aim to uncover novel methods for optimising ansätze that represent fermionic wavefunctions.

This led us to the work by Yordanov *et al* [9], which demonstrates that excitation operators can be re-expressed in terms of controlled rotations, and the work by Cowtan *et al.* [10], which shows that commuting sets of Pauli gadgets can be diagonalised and optimally resynthesised. Throughout this thesis, we were able to demonstrate the correspondence between excitation operators and controlled rotations in the ZX calculus, laying the groundwork for future optimisation strategies.

While quantum chemistry is anticipated to be a principal application of quantum computing, it remains an area with limited engagement among Master's level researchers in Chemistry. Furthermore, the ZX calculus, despite its immense promise as a next-generation framework for studying quantum computing, has seen relatively low usage by quantum chemists. Therefore, we hope that this thesis, along with the tools developed herein, will help to lower the barrier to entry for future Master's and PhD students interested in quantum computing. By providing a solid theoretical foundation and practical insights, we aim to facilitate a smoother transition and foster greater interest in this rapidly developing field.

To summarise: we aim to identify a generalised representation of excitation operators within the ZX calculus to gain insights into the nature of correlations in molecular quantum systems. Then, using these insights, we seek to rationalise the varying outputs of VQE algorithms that yield the same energy and discover more efficient implementations of UPS ansätze. Finally, we aim to lower the barrier to entry for quantum computing in the context of quantum chemistry.

1.2 Electronic Structure Theory

Electronic Structure Problem

The main interest of electronic structure theory is finding approximate solutions to the eigenvalue equation of the full molecular Hamiltonian. Specifically, we seek solutions to the non-relativistic time-independent Schrödinger equation.

The full molecular Hamiltonian describes all of the interactions within a system of N interacting electrons and M nuclei. We are able to simplify the problem to an electronic one using the Born-Oppenheimer approximation. Motivated by the large difference in mass of electrons and nuclei, we can approximate nuclei as stationary on the timescale of electronic motion such that the electronic wavefunction depends only parametrically on the nuclear coordinates. Within this approximation, the nuclear kinetic energy term can be neglected and the nuclear repulsive term is considered to be constant. Following this, we obtain the electronic Hamiltonian for N electrons.

$$H = -\sum_{i=1}^{N} \frac{1}{2}\nabla_i^2 - \sum_{i=1}^{N}\sum_{j=1}^{M} \frac{Z_j}{|r_i - R_j|} + \sum_{i=1}^{N}\sum_{j>i}^{N} \frac{1}{|r_i - r_j|}$$

Figure 1.1: Electronic molecular Hamiltonian in atomic units.

The first term corresponds to the kinetic energy of the N electrons in the system, the second term corresponds to the pairwise attractive Coulombic interactions between the N electrons and M nuclei and the final term corresponds to the repulsive Coulombic interactions between N electrons in the system. Throughout the remainder of this text, we concern ourselves only with the electronic Hamiltonian, simply referring to it as the Hamiltonian, H. The solution to the eigenvalue equation involving the electronic Hamiltonian is the electronic wavefunction, which depends only parametrically on the nuclear coordinates. It is solved for fixed nuclear coordinates, such that different arrangements of nuclei yields different functions of the electronic coordinates. The total molecular energy can be calculated by solving the electronic Schrödinger equation and including a constant nuclear term.

Many-Electron Wavefunctions

The many-electron wavefunction, which describes all the electrons in given molecular system, must satisfy the Pauli principle. This is an independent postulate of quantum mechanics that requires the many-electron wavefunction to be antisymmetric with respect to the exchange of any two fermions.

A spatial molecular orbital is defined as a one-particle function of the position vector, spanning the whole molecule. The spatial orbitals form an orthonormal set $\{\psi_i(\mathbf{r})\}$, which if complete can be used to expand any arbitrary single-particle molecular wavefunction, that is, an arbitrary single-particle function of the position vector. In practice, only a finite set of such orbitals is available to us, spanning only a subspace of the complete space. Hence, wavefunctions expanded using this finite set are described as being 'exact' only within the subspace that they span.

We now introduce the spin orbitals $\{\phi_i(\mathbf{x})\}$, that is, the set of functions of the composite coordinate $\mathbf{x}$, which describes both the spin and spatial distribution of an electron. Given a set of K spatial orbitals, we can construct $2K$ spin orbitals by taking their product with the orthonormal spin functions $\alpha(\omega)$ and $\beta(\omega)$. Whilst the Hamiltonian operator makes no reference to spin, it is a necessary component when constructing many-electron wavefunctions in order to correctly antisymmetrise the wavefunction with respect to fermion exchange. Constructing the antisymmetric many-electron wavefunction from a finite set of spin orbitals amounts to taking the appropriate linear combinations of symmetric products of N spin orbitals. A general procedure for this is achieved by constructing a Slater determinant from the finite set of spin orbitals, where each row relates to the electron coordinate $\mathbf{x_n}$ and each column corresponds to a particular spin orbital ϕ_i [13].

$$\psi(\mathbf{x}_1, \mathbf{x}_2) = \frac{1}{\sqrt{N!}} \begin{vmatrix} \phi_i(\mathbf{x}_1) & \phi_j(\mathbf{x}_1) & \dots & \phi_k(\mathbf{x}_1) \\ \phi_i(\mathbf{x}_2) & \phi_j(\mathbf{x}_2) & \dots & \phi_k(\mathbf{x}_2) \\ \vdots & \vdots & & \vdots \\ \phi_i(\mathbf{x}_N) & \phi_j(\mathbf{x}_N) & \dots & \phi_k(\mathbf{x}_N) \end{vmatrix}$$

Figure 1.2: Slater determinant representing an antisymmetrised N-electron wavefunction.

By constructing Slater determinants and antisymmetrising the many-electron wavefunction to meet the requirements of the Pauli principle, we have incorporated exchange correlation, in that, the motion of any two electrons with parallel spins is now correlated [13].

The Hartree-Fock method yields a set of orthonormal spin orbitals, which when used to construct a single Slater determinant, gives the best variational approximation to the ground state of a system [13]. By treating electron-electron repulsion in an average way, the Hartree-Fock approximation allows us to iteratively solve the Hartree-Fock equation for spin orbitals until they become the same as the eigenfunctions of the Fock operator. This is known as the Self-Consistent Field (SCF) method and is an elegant starting point for finding approximate solutions to the many-electron wavefunction.

Second Quantisation

In second quantisation, both observables and states are represented by creation and annihilation operators. Unlike the standard formulation of quantum mechanics, these operators inherently incorporate Bose or Fermi statistics, eliminating the need to track symmetrised or antisymmetrised products of single-particle wavefunctions. Put differently, the antisymmetry of an electronic wavefunction follows from the algebra of these operators, which greatly simplifyies the discussion of many identical interacting fermions [14], [15].

The Fock space is a linear abstract vector space spanned by N orthonormal occupation number vectors, each representing a single Slater determinant [14]. Hence, given a basis of N spin orbitals we can construct 2^N single Slater determinants, each corresponding to a single occupation number vector in the full Fock space. The occupation number representation of fermionic states is succinctly denoted in Dirac notation as below, where the occupation number f_j is 1 if spin orbital j is occupied, and 0 if spin orbital j is unnoccupied.

$$|\psi\rangle = |f_{n-1}\ f_{n-2} \dots f_1\ f_0\rangle \qquad \text{where } f_j \in 0, 1$$

Whilst there is a one-to-one mapping between Slater determinants with canonically ordered spin orbitals and the occupation number vectors in the Fock space, it is important to distinguish between the two since, unlike the Slater determinants, the occupation number vectors have no spatial structure and are simply vectors in an abstract vector space [14].

Operators in second quantisation are constructed from the creation and annhilation operators $a_j^\dagger$ and a_j, where the subscripts i and j denote the spin orbital. $a_j^\dagger$ and a_j are one another's Hermitian adjoints, and are not self-adjoint [14]. Due to the fermionic exchange anti-symmetry imposed by the Pauli principle, the action of the creation and annhilation operators introduces a phase to the state that depends on the parity of the spin orbitals preceding the target spin orbital. This phase factor is automatically kept track of by the creation and annhilation operators' anticommutation relations [14].

$$\{\hat{a}_j, \hat{a}_k\} = 0 \qquad \{\hat{a}_j^\dagger, \hat{a}_k^\dagger\} = 0 \qquad \{\hat{a}_j, \hat{a}_k^\dagger\} = \delta_{jk}\hat{1}$$

Figure 1.3: Anticommutation relations of the creation and annhilation operators.

The Hamiltonian in second quantisation can be expressed as follows, where the one-body matrix element h_{ij} corresponds to the kinetic energy of an electron and its interaction energy with the nuclei, and the two-body matrix element h_{ijkl} corresponds to the repulsive interaction between electrons i and j.

$$\hat{H} = \sum_{ij} h_{ij} a_i^\dagger a_j + \frac{1}{2} \sum_{ijkl} h_{ijkl} a_i^\dagger a_j^\dagger a_k a_l + h_{\mathrm{Nu}}$$

These matrix elements are then computed classically, allowing us to simulate only the inherently quantum aspects of the problem on a quantum computer.

$$h_{ij} = \int_{-\infty}^{\infty} \psi_{i(x_1)}^* \left(-\frac{1}{2}\nabla^2 + \hat{V}_{(x_1)} \right) \psi_{j(x_1)} \, d^3x_1$$

$$h_{ijkl} = \int_{-\infty}^{\infty} \int_{-\infty}^{\infty} \psi_{i(x_1)}^* \psi_{j(x_2)}^* \left(\frac{1}{|x_1 - x_2|} \right) \psi_{k(x_2)} \psi_{l(x_1)} \, d^3x_1 d^3x_2$$

1.3 Fundamentals of Quantum Computating

The central concept that enables gate-based quantum computation to represrent exponentially scaling fermionic states with polynomially scaling quantum resources is its ability to encode and manipulate superpositions of states. In this section, we provide an introduction to qubits and basic quantum gates.

Introduction to Qubits

Classical computation encodes information using binary strings formed from the computational basis states 0 and 1. Thus, given n classical bits, we can encode 2^n binary strings. In contrast, information on a quantum computer is encoded using two quantum states, corresponding to vectors in a two-dimensional complex Hilert space $\mathbb{C}$. The $|0\rangle$ and $|1\rangle$ states, known as the Z computational basis, form the standard computational basis for encoding information on a quantum computer.

Figure 1.4: Z computational basis states.

An arbitrary qubit state $|\psi\rangle$ can be described as a complex linear combination of the computational basis states, $|\psi\rangle = \alpha\,|0\rangle + \beta\,|1\rangle$, provided that the qubit state is normalised. In other words we require two complex numbers, or four real numbers, to describe an arbitrary qubit state. Since only the relative phase between the basis states is directly measureable, there is a redundancy in this description that allows us to represent an arbitrary qubit state using only three real numbers.

By taking advantage of this redundancy, we can derive a three-dimensional representation of an arbitrary qubit state, known as the Bloch sphere. Note that opposite points on the Bloch sphere correspond to mutually orthonal states, as in Figure 1.4 in which we have represented the Z computational basis states.

We could have chosen to form our computational basis with any pair of orthonormal states. For instance, we define the X basis states as follows.

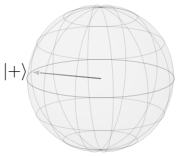

$$= \frac{|0\rangle + |1\rangle}{\sqrt{2}}$$

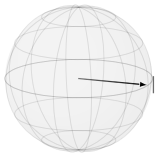

$$= \frac{|0\rangle - |1\rangle}{\sqrt{2}}$$

Figure 1.5: Computational X basis states.

In theory, a qubit can exist in an infinite number of states, however, upon measuring with respect to a particular basis, the qubit state collapses into one computational basis state, or the other. This result is known more formally as the *no-cloning theorem*, which states that we cannot create indentical and independent copies of an arbitrary qubit state, as this would involve first measuring that state.

Multiple-Qubit States

Let us now consider systems consisting of multiple qubits. Similarly to how n classical bits give rise to 2^n binary strings, we have that, n qubits give rise to 2^n basis states. These basis states are formed by taking the Kronecker product. For instance, a two-qubit system gives rise to the four following basis states.

$$|00\rangle = |0\rangle \otimes |0\rangle \qquad |01\rangle = |0\rangle \otimes |1\rangle \qquad |10\rangle = |1\rangle \otimes |0\rangle \qquad |11\rangle = |1\rangle \otimes |1\rangle$$

Figure 1.6: The four basis states associated with a two-qubit system.

An arbitrary n-qubit *state vector*, describing the state of the entire system, can be formed by taking a complex linear combination of the 2^n basis states. Therefore, in order to fully describe an arbitrary n-qubit state vector, we need to specify 2^n complex coefficients. In the case of a two-qubit system, we have the following.

$$|\psi\rangle = \alpha\,|00\rangle + \beta\,|01\rangle + \gamma\,|10\rangle + \delta\,|11\rangle$$

$$\text{where} \quad \alpha,\, \beta,\, \gamma,\, \delta \in \mathbb{C}$$

Introduction to Quantum Gates

By definition, quantum gates correspond to unitary transformations, $U^{-1} = U^{\dagger}$ [16]. In other words, any quantum gate corresponds to a square unitary matrix that conserves the complex inner product of the state it acts on. Consequently, quantum gates can be viewed as rotations of the qubit state vector in Hilbert space.

Let us now introduce the most fundamental quantum gates: the Pauli gates. The Pauli gates are described by the 2×2 Pauli matrices and rotate an arbitrary qubit state by π radians about their respective axes.

$$I = \begin{pmatrix} 1 & 0 \\ 0 & 1 \end{pmatrix} \qquad X = \begin{pmatrix} 0 & 1 \\ 1 & 0 \end{pmatrix} \qquad Y = \begin{pmatrix} 0 & -i \\ i & 0 \end{pmatrix} \qquad Z = \begin{pmatrix} 1 & 0 \\ 0 & -1 \end{pmatrix}$$

Figure 1.7: The Pauli matrices corresponding to the Pauli gates.

The Pauli X gate is the quantum analogue of the classical NOT gate in that it maps $|0\rangle \leftrightarrow |1\rangle$. Importantly, the Pauli X differs from its classical counterpart in that it can act on any arbitrary qubit state. Similarly, we have that the Pauli Z gate maps $|+\rangle \leftrightarrow |-\rangle$, but can also act on any arbitrary qubit state.

The Hadamard gate is a member of the Clifford group that maps $|0\rangle \leftrightarrow |+\rangle$ and $|1\rangle \leftrightarrow |-\rangle$. Therefore, the Hadamard gate can be viewed as a rotation of the Bloch sphere π radians about the line bisecting the z and x axes.

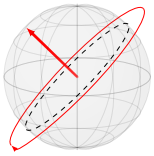

$$= \frac{1}{\sqrt{2}} \begin{pmatrix} 1 & 1 \\ 1 & -1 \end{pmatrix}$$

Figure 1.8: Bloch sphere representation of the Hadamard gate.

Since the Pauli gates and the Hadamard gate each correspond to unitary and Hermitian matrices, it follows that they are also self-inverse. Consequently, successively applying any of these gates is equivalent to applying the identity matrix I.

The $R_Z(\theta)$ and $R_X(\theta)$ rotation gates correspond to rotations of the Bloch sphere by some angle θ about the Z and X axes respectively.

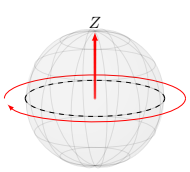

$$= \begin{pmatrix} 1 & 0 \\ 0 & e^{i\theta} \end{pmatrix}$$

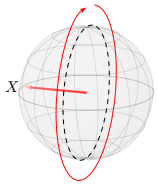

$$= \begin{pmatrix} 1+e^{i\theta} & 1-e^{i\theta} \\ 1-e^{i\theta} & 1+e^{i\theta} \end{pmatrix}$$

Figure 1.9: Bloch sphere representations of arbitrary Z and X rotations.

Multiple-Qubit Gates

The CNOT gate is a two-qubit member of the Clifford group which we can use to entangle qubits. Consider a two-qubit state of the form $|\alpha\rangle \otimes |\beta\rangle$. Taking the first qubit (α) to be the control, and the second qubit (β) to be the target, we define the CNOT gate as the gate that maps $|\alpha\rangle \otimes |\beta\rangle \to |\alpha\rangle \otimes |\alpha \oplus \beta\rangle$. That is, the CNOT gate applies the Pauli X gate to the target qubit *iff* the control qubit is in the $|1\rangle$ state. The CNOT gate acts on the two-qubit basis states (1.6) as follows.

$$|00\rangle \to |00\rangle \qquad |01\rangle \to |01\rangle \qquad |10\rangle \to |11\rangle \qquad |11\rangle \to |10\rangle$$

In this way the CNOT gate is the quantum generalisation of the classical XOR gate. We define the two matrices corresponding to the two CNOT gates, with the first qubit being the control and the second qubit being the target, and *vice versa*.

$$\mathrm{CNOT}^{c=0}_{t=1} = \begin{pmatrix} 1 & 0 & 0 & 0 \\ 0 & 1 & 0 & 0 \\ 0 & 0 & 0 & 1 \\ 0 & 0 & 1 & 0 \end{pmatrix} \qquad \mathrm{CNOT}^{c=1}_{t=0} = \begin{pmatrix} 1 & 0 & 0 & 0 \\ 0 & 0 & 0 & 1 \\ 0 & 0 & 1 & 0 \\ 0 & 1 & 0 & 0 \end{pmatrix}$$

Figure 1.10: Matrix definitions of the CNOT gate.

The CNOT gate can be used to entangle two qubits when the control qubit exists in a superposition of states. For instance, applying CNOT gate to the $|+0\rangle$ state, letting the first qubit be the control qubit ($|+\rangle$), yields the following Bell state.

$$\mathrm{CNOT}\,|+0\rangle = \frac{|00\rangle + |11\rangle}{\sqrt{2}}$$

1.4 The Variational Quantum Eigensolver

In this chapter, we introduce the *Variational Quantum Eigensolver (VQE)* algorithm, a particular class of variational quantum algorithms used to estimate the ground state energy of molecular systems. The research presented in this thesis is conducted within this framework. As providing an overview of the VQE algorithm, we introduce the fundamentals of quantum computing and the *Unitary Product State (UPS) ansatz* used to represent fermionic wavefunctions on quantum devices.

The VQE algorithm consists of a quantum subroutine, a *Parametrised Quantum Circuit (PQC)*, that implements some UPS ansatz, and a classical subroutine that classically optimises the ansatz until it converges to the best approximation of the true ground state. PQCs are similar to classical neural networks in concept, but by definition, correspond to $2^n \times 2^n$ unitary maps, where n is the number of qubits, and hence have the same number of inputs as outputs [3].

The input state for the PQC is the reference state that the unitary operator $U(\boldsymbol{\theta})$ acts on, which in the case of the single Slater determinant Hartree-Fock state, is encoded as a pure quantum state $|\psi_0\rangle$. The output of the PQC is then an entangled state, that is, some linear combination of vectors in the Fock space, that captures the correlation present in true ground state of the molecular system of interest.

Upon measuring the PQC output state, it collapses into a single vector in the Fock space, with a probability defined by that vector's weight in the UPS ansatz. The quantum subroutine computes the energy expectation value of the UPS ansatz via a quantum circuit consisting of the PQC and the Hamiltonian for the system.

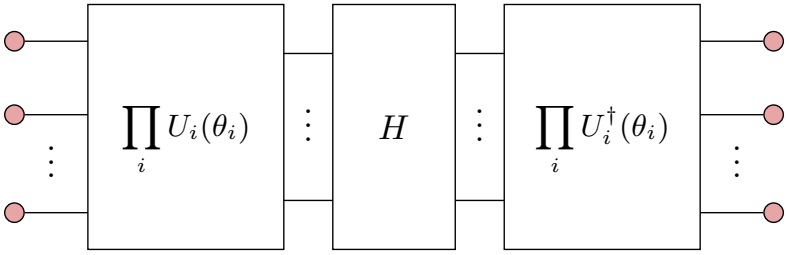

$$E(\boldsymbol{\theta}) = \langle 0 | U^\dagger(\boldsymbol{\theta}) H U(\boldsymbol{\theta}) | 0 \rangle$$

For the purposes of this thesis, we are interested in a variant of the VQE algorithm developed by Burton *et al* [5] known as the *Discretely and Continuously Optimised Variational Quantum Eigensolver (DISCO-VQE)*. We implement a fermionic state on a quantum device as a sequence of quantum gates representing unitary excitation operators that act on some reference state. The DISCO-VQE algorithm then finds approximate solutions to the fermionic ground state by both (*discretely*) optimising the sequence of fermionic excitation operators, chosen from a finite operator pool, and (*continuously*) optimising their parameters. This allows us to parametrically explore the Hilbert space of possible quantum states until we find a good approximation of the true fermionic ground state [17]. The DISCO-VQE algorithm, therefore, discovers accurate representations of fermionic wavefunctions using a minimal number of parameters [5].

Unitary Product State Ansatz

As suggested by Peruzzo *et al* [18], the UCC formulation of a wavefunction can be efficiently implemented on a quantum device in terms of quantum gates. We refer to the UCC ansatz $|\psi_{\mathrm{UCC}}(\boldsymbol{\theta})\rangle$ as some unitary excitation operator $U_{\mathrm{UCC}}(\boldsymbol{\theta})$ acting on a reference state, usually a single-Slater determinant Hartree-Fock state $|\psi_0\rangle$ obtained via the self-consistent field method.

$$|\psi_{\mathrm{UCC}}(\boldsymbol{\theta})\rangle = U_{\mathrm{UCC}}(\boldsymbol{\theta})\,|\psi_0\rangle = e^{\hat{T}(\boldsymbol{\theta})-\hat{T}^\dagger(\boldsymbol{\theta})}\,|\psi_0\rangle$$

The operator $\hat{T}(\boldsymbol{\theta})$ is a linear combination of fermionic second-quantised excitation operators, parametrised by coupled cluster amplitudes $\boldsymbol{\theta}$. The exponential of the anti-Hermitian operator $\hat{T}(\boldsymbol{\theta}) - \hat{T}^\dagger(\boldsymbol{\theta})$ is therefore, by definition, unitary.

$$\hat{T}(\boldsymbol{\theta}) - \hat{T}^\dagger(\boldsymbol{\theta}) = \sum_{i,a} \theta_i^a (a_i^\dagger a_a - a_a^\dagger a_i) + \sum_{i,j,a,b} \theta_{ij}^{ab} (a_i^\dagger a_j^\dagger a_a a_b - a_a^\dagger a_b^\dagger a_i a_j) + \dots$$

Where i, j indexes occupied spin orbitals and a, b indexes virtual, or unoccupied, spin orbitals. The *Singles-Doubles* formulation of the UCC ansatz has been shown by Evangelista *et al* to exactly parametrise any state, [19]. However, since the terms of the unitary operator $U_{\mathrm{UCC}}(\boldsymbol{\theta})$ do not commute, it cannot be directly implemented

on a quantum computer. Instead, by invoking the Trotter formula to approximate the unitary with a single Trotter step, since our focus is on the NISQ setting [10], we define the *Unitary Product State (UPS)* ansatz $|\psi(\boldsymbol{\theta})\rangle$ as the following product of k parametrised unitary excitation operators [5].

$$|\psi(\boldsymbol{\theta})\rangle = \prod_{m=1}^{k} U_m(\theta_m) |\psi_0\rangle \qquad U_m(\theta_m) = e^{\theta_m(\tau_m - \tau_m^\dagger)}$$

Figure 1.11: Parametrised k-UPS ansatz.

Where m indexes all possible excitations and $\tau_m - \tau_m^\dagger$ corresponds to anti-Hermitian fermionic excitation operators in second quantisation. For the remainder of this thesis, we refer to fermionic excitation operators as the the exponentials of these anti-Hermitian operators, $U_m(\theta_m)$. As these fermionic excitation operators are derived from second-quantised operators, they preserve the fermionic anti-symmetry and particle number of the reference state [5].

The operators are then mapped to quantum gates using the Jordan-Wigner transformation (see Chapter 5) before being implemented on a quantum device. Within the DISCO-VQE framework, we consider only generalised *single* (one-body) and *double* (two-body) fermionic excitation (operators), which, as shown by Burton *et al* [5], achieves universality provided that we combine enough suitably-ordered one-body and two-body excitation operators. In other words, the UPS ansatz is sufficient to represent any vector in the Hilbert space.

Chapter 2

ZX Calculus

In this chapter, we introduce the ZX calculus, a diagrammatic language for reasoning about quantum processes first introduced by Coecke *et al* [11]. The ZX calculus is *universal* in that it can represent any linear map (any complex matrix of dimension $2^n \times 2^m$). In other words, any equation involving linear maps that is derivable in multilinear algebra can also be derived in the ZX calculus through its rewrite rules [20]. Another important property of the ZX calculus is its *soundness*, by which we mean that the diagrammatic rewrite rules preserve the underlying semantics of the linear map represented by a ZX diagram [21]. We aim to use the ZX calculus to study UPS ansätze (Section 1.4) representing fermionic states, demonstrating its usefulness as an alternative perspective on the theory underlying the simulation of quantum systems.

This thesis uses the scalar-free ZX calculus. That is, the derivations in this thesis are correct up to some global non-zero scalar factor. All equal signs should, therefore, be interpreted as 'equal up to a global phase'. This is done for convenience, in a similar way to how we sometimes work with unnormalised wavefunctions. Recalling that the matrix representing our quantum circuit M is proportional to some unitary, $M^{-1} = M^\dagger$, we can later efficiently compute the scalar factor [21].

Remark – *All of the definitions in this chapter also hold for their colour-swapped counterparts, which we have chosen to omit for brevity.*

2.1 Generators

By sequentially or horizontally composing the *Z Spider* (green) and *X Spider* (red) generators, we can construct undirected multigraphs known as ZX diagrams [21]. That is, graphs that allow multiple edges between vertices. Since *only connectivity matters* in the ZX calculus, a valid ZX diagram can be arbitrarily deformed (d), provided that the order of inputs and outputs is preserved.

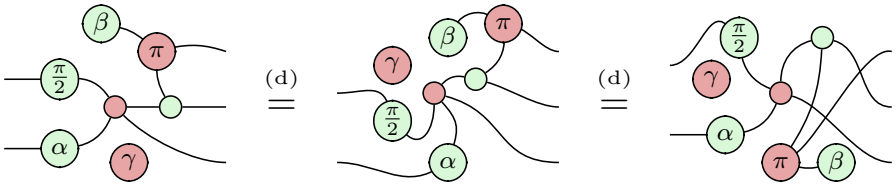

Figure 2.1: Three equivalent ZX diagrams (*only connectivity matters*).

Notation – *We interpret the flow of time left to right. Hence, the wires on the left refer to inputs and the wires on the right refer to outputs.*

Z Spiders (green) are defined with respect to the Z eigenbasis (1.4). A Z Spider with n inputs and m outputs represents the following linear map.

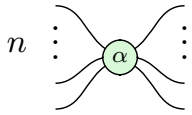

$$= |0\rangle^{\otimes m} \langle 0|^{\otimes n} + e^{i\alpha} |1\rangle^{\otimes m} \langle 1|^{\otimes n}$$

Figure 2.2: Interpretation of a Z Spider as a linear map.

X Spiders (red), are defined with respect to the X eigenbasis (1.5).

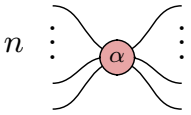

$$= |+\rangle^{\otimes m} \langle +|^{\otimes n} + e^{i\alpha} |-\rangle^{\otimes m} \langle -|^{\otimes n}$$

Figure 2.3: Interpretation of an X Spider as a linear map.

We can represent the Z eigenstates using an X spider with a phase of 0 or π.

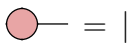

$$= |+\rangle + |-\rangle = \sqrt{2}\,|0\rangle$$

Figure 2.4: $|0\rangle$ eigenstate

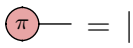

$$= |+\rangle - |-\rangle = \sqrt{2}\,|1\rangle$$

Figure 2.5: $|1\rangle$ eigenstate

Similarly, we represent the X eigenstates using the corresponding Z spiders.

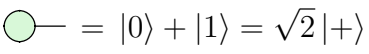

Figure 2.6: $|+\rangle$ eigenstate

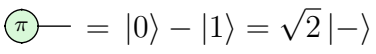

Figure 2.7: $|-\rangle$ eigenstate

Arbitrary single-qubit rotations (1.9) in the Z basis are represented by a Z Spider with a single input and a single output. Similarly, we have that the corresponding rotation in the X basis is represented by an X spider. We can view these as rotations of the Bloch sphere.

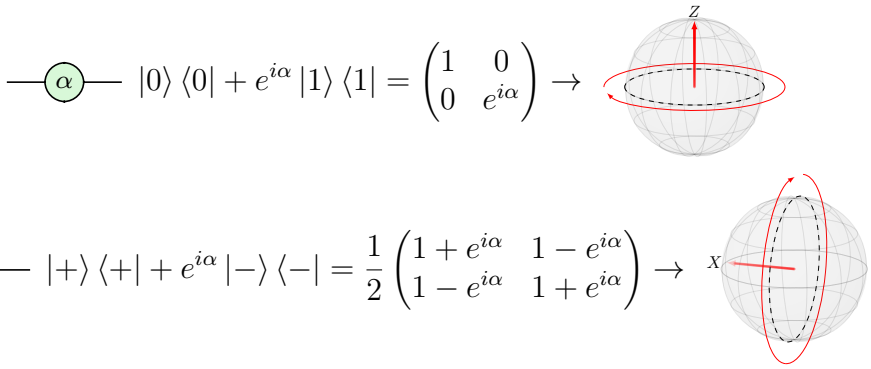

We can recover the Pauli Z and Pauli X matrices (1.7) by setting $\alpha = \pi$.

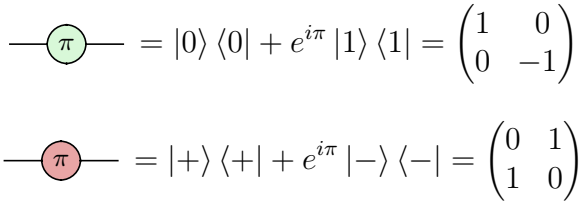

Figure 2.8: Pauli Z and X gates in the ZX calculus.

Composition

To calculate the matrix of a ZX diagram consisting of sequentially composed spiders, we take the matrix product. Note that the order of operation of matrix multiplication is the reverse of how we have defined it for ZX diagrams.

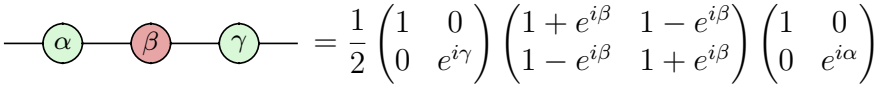

In contrast, by composing spiders in parallel, we obtain the tensor product. Note that the order of operation should be interpreted from top to bottom.

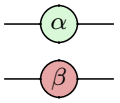

$$= \frac{1}{2}\begin{pmatrix}1 & 0\\ 0 & e^{i\alpha}\end{pmatrix} \otimes \begin{pmatrix}1+e^{i\beta} & 1-e^{i\beta}\\ 1-e^{i\beta} & 1+e^{i\beta}\end{pmatrix}$$

The CNOT gate (1.10) is represented in the ZX calculus by a Z spider (control qubit) and an X spider (target qubit). We can arbitrarily deform the diagram and decompose it into matrix and tensor products as follows.

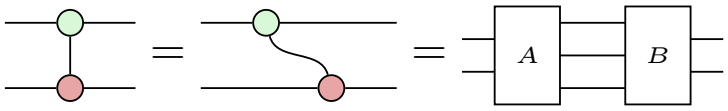

We can calculate matrix A, consisting of a single-input and two-output Z Spider (4×2 matrix) and an empty wire (identity matrix), by taking the tensor product.

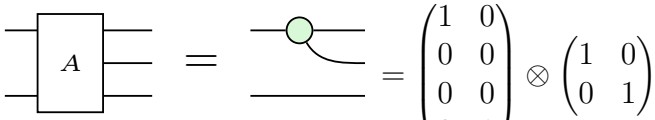

$$= \begin{pmatrix}1 & 0\\ 0 & 0\\ 0 & 0\\ 0 & 1\end{pmatrix} \otimes \begin{pmatrix}1 & 0\\ 0 & 1\end{pmatrix}$$

Similarly, to calculate the matrix B, we take the following tensor product.

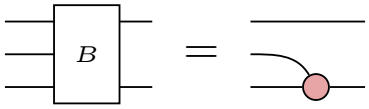

$$= \begin{pmatrix}1 & 0\\ 0 & 1\end{pmatrix} \otimes \frac{1}{\sqrt{2}}\begin{pmatrix}1 & 0 & 0 & 1\\ 0 & 1 & 1 & 0\end{pmatrix}$$

We can then calculate the CNOT matrix by taking the matrix product of matrix A and matrix B as follows (up to a global scalar factor of $1/\sqrt{2}$).

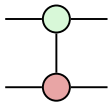

$$= \left[\begin{pmatrix}1 & 0\\ 0 & 1\end{pmatrix} \otimes \frac{1}{\sqrt{2}}\begin{pmatrix}1 & 0 & 0 & 1\\ 0 & 1 & 1 & 0\end{pmatrix}\right]\left[\begin{pmatrix}1 & 0\\ 0 & 0\\ 0 & 0\\ 0 & 1\end{pmatrix} \otimes \begin{pmatrix}1 & 0\\ 0 & 1\end{pmatrix}\right] \simeq \begin{pmatrix}1 & 0 & 0 & 0\\ 0 & 1 & 0 & 0\\ 0 & 0 & 0 & 1\\ 0 & 0 & 1 & 0\end{pmatrix}$$

Had we chosen to make the first qubit the target and the second qubit the control, we would have instead obtained the following matrix.

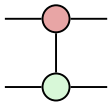

$$= \left[\frac{1}{\sqrt{2}}\begin{pmatrix}1&0&0&1\\0&1&1&0\end{pmatrix} \otimes \begin{pmatrix}1&0\\0&1\end{pmatrix}\right]\left[\begin{pmatrix}1&0\\0&1\end{pmatrix} \otimes \begin{pmatrix}1&0\\0&0\\0&0\\0&1\end{pmatrix}\right] \simeq \begin{pmatrix}1&0&0&0\\0&0&0&1\\0&0&1&0\\0&1&0&0\end{pmatrix}$$

Hadamard Generator

Up to a global phase, an arbitrary single qubit gate U can be viewed as a rotation of the Bloch sphere about some axis. Therefore, we can decompose U using Euler angles to represent it as three successive rotations [21].

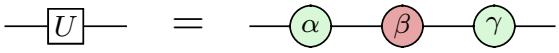

The Hadamard gate H (1.8) corresponds to a rotation of the Bloch sphere π radians about the line bisecting the X and Z axes. Up to a global phase of $\exp\left(-i\frac{\pi}{4}\right)$, it can be decomposed into three successive rotations by choosing $\alpha = \beta = \gamma = \frac{\pi}{2}$.

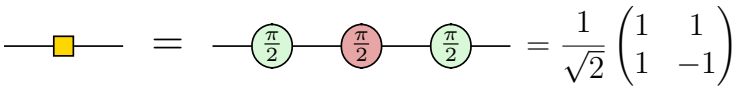

$$= \frac{1}{\sqrt{2}}\begin{pmatrix}1&1\\1&-1\end{pmatrix}$$

Recall that the Hadamard gate is the member of the Clifford group that switches between the Z and X bases (1.8). Hence, diagrammatically, applying Hadamard generators to all of the legs of a spider changes the colour of the spider.

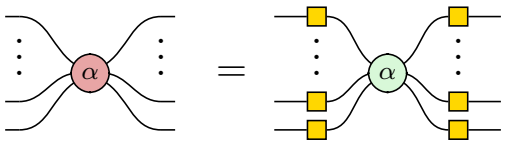

The CZ gate applies the Pauli Z gate to the target qubit *iff* the control qubit is in the $|1\rangle$ state. It is diagonal in the Z basis and has a symmetric representation in the ZX calculus. It can be derived by conjugating the target of the CNOT gate with Hadamards, then applying the Hadamard commutation rule (2.14).

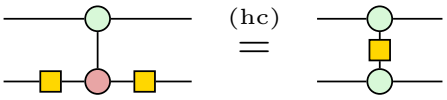

Figure 2.9: The CZ gate in the ZX calculus.

2.2 Rewrite Rules

Notation – *We refer to the rules by some shorthand notation above equal signs. Note that this could refer to applying the rule in either direction.*

Spider Fusion

The most fundamental rule of the ZX calculus is the *spider fusion rule* (f). It states that spiders of the same colour connected by one or more wires fuse and their phases add modulo 2π [21].

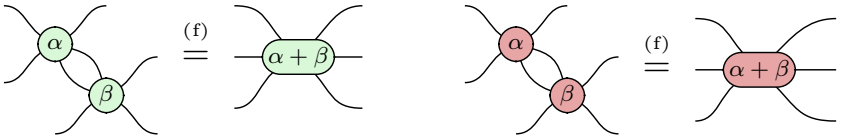

Figure 2.10: Spider fusion rule for Z spiders (left) and X spiders (right).

It is the generalisation of adding the phases of successive rotations of the Bloch sphere. We can use this rule to show that Z rotations commute through CNOT controls, and that X rotations commute through CNOT targets.

Identity Removal

The *identity rule* (id) states that any two-legged spider with no phase ($\alpha = 0$) is equivalent to a rotation by 0 radians, or identity.

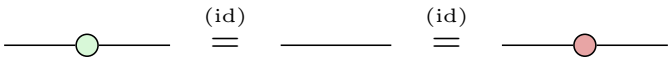

Figure 2.11: Identity removal rule.

Combining this with the spider fusion rule (2.10), we see that two successive rotations with opposite phases is equivalent to an empty wire.

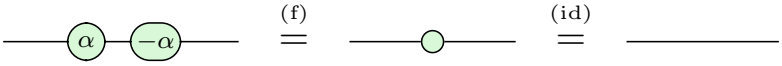

State Copy and π Copy Rules

We can depict the Z and X eigenstates (2.5, 2.7) by assigning a phase of π multiplied by a Boolean variable a (0 or 1) to an X or Z spider, respectively [21].

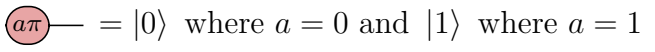

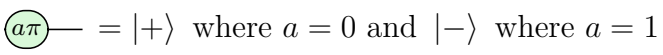

The π *copy rule* (c) states that when a Pauli Z or Pauli X gate is pushed through a spider of the opposite colour, it is copied on all other legs and negates the spider's phase. A similar *state copy rule* (c) applies to the Z and X eigenstates.

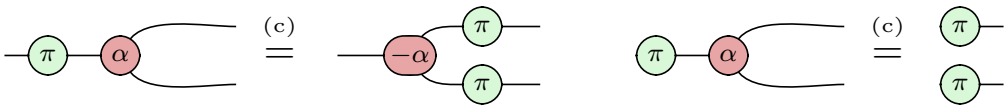

Figure 2.12: π copy (left) and state copy (right) rules for Pauli Z gate and Z eigenstates.

Hadamard Rules

Using that the Hadamard gate is both unitary and Hermitian, we define the *Hadamard self-inverse rule* (hi) as follows.

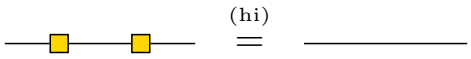

Figure 2.13: Hadamard self-inverse rule.

Recalling that the Hadamard generator changes the colour of a spider and is self-inverse, we define the *Hadamard commutation rule* (hc).

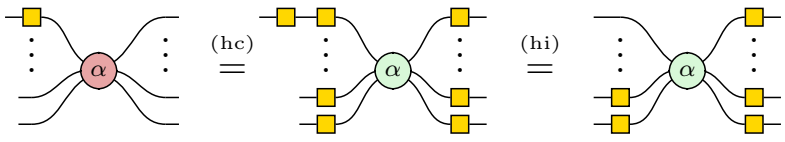

Figure 2.14: Hadamard commutation rule.

Bialgebra Rule

Using the spider fusion rule (2.10), we can show that a spider with two inputs and one output behaves like a classical XOR gate when applied to the eigenstates of the

same basis. Whilst using the state copy rule (2.12), we can show that a spider with one input and two outputs behaves like a classical COPY gate when applied to the eigenstates of the *opposite* basis.

Figure 2.15: XOR gate (left) and COPY gate (right) with respect to the Z eigenstates.

The natural commutation relation of the classical XOR and COPY gates, implies the *bialgebra rule* (*ba*). By successively applying the two-input/two-output case, we can generalise to any number of inputs and outputs.

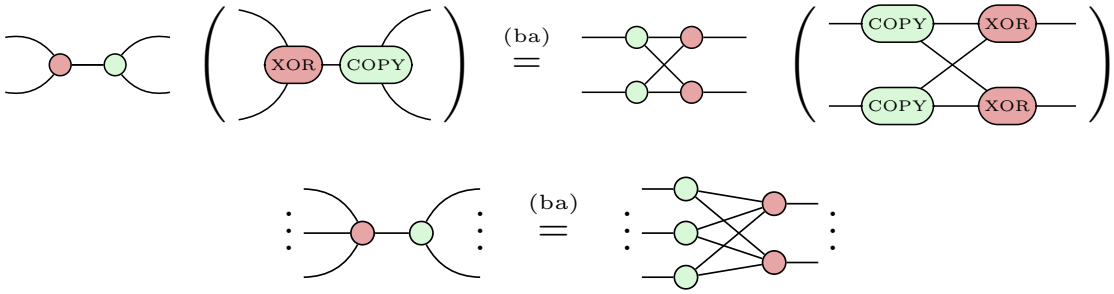

Figure 2.16: The bialgebra rule.

Hopf Rule

Like with the bialgebra rule, our motivation for this rule stems from the behaviour of the classical XOR and COPY gates. Since copying two bits then taking their XOR invariably yields 0, we define the *Hopf rule* (*hpf*).

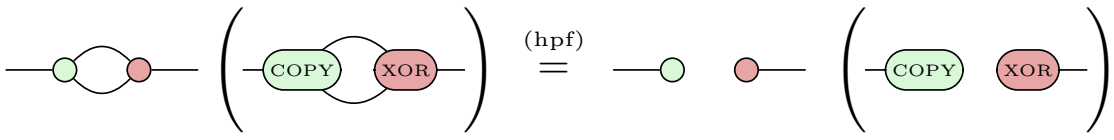

Figure 2.17: The Hopf rule.

Recall that the CNOT gate is both unitary and Hermitian, and therefore, self-inverse. The Hopf rule allows us to prove this diagrammatically as follows.

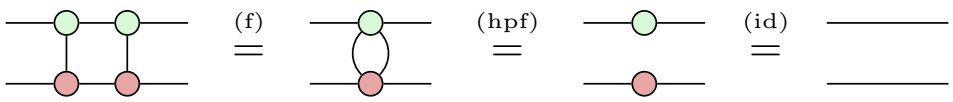

2.3 Clifford Conjugation

The ZX calculus is a diagrammatic language that makes use of the complementary observables in the Z and X bases. Since both of these bases are Hermitian, we can arbitrarily deform their wires as we see fit. For instance, it is easy to show that the Pauli Z gate (Z spider with phase π) is Hermitian, $Z = Z^\dagger$, by finding its transpose (converting its inputs into outputs and *vice verse*), then taking its complex conjugate (negating its phase $\pi \to -\pi = \pi$).

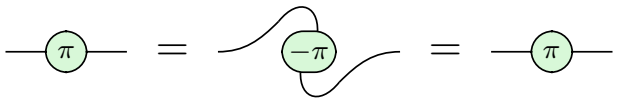

The Y basis, unlike the Z and X bases, is *not* Hermitian. Therefore, converting the inputs of a Y *Spider* into outputs and *vice verse* does *not* yield its transpose. We define rotations in the Y basis with the following Clifford conjugations [3].

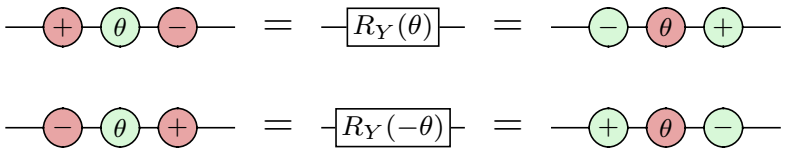

Figure 2.18: Conjugation of generators in the Z and X bases into the Y basis.

The single-qubit Clifford gates, $R_Z\left(\frac{\pi}{2}\right)$, $R_Z\left(\frac{3\pi}{2}\right)$, $R_X\left(\frac{\pi}{2}\right)$ and $R_X\left(\frac{\pi}{2}\right)$, as defined in Grier *et al* [22], are represented as follows in the ZX calculus.

Figure 2.19: Definition of the single-qubit Clifford gates.

Using the fact that the Clifford gates are unitary $C^{-1} = C^\dagger$, we expand our definition of the Y rotation to obtain the following commutation relations [3].

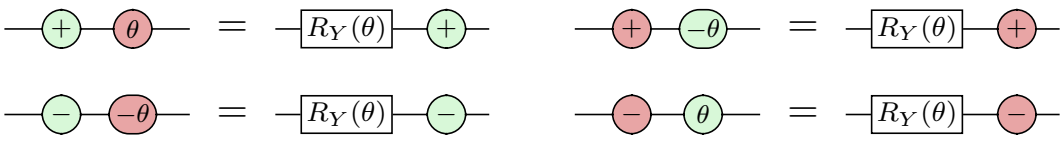

Figure 2.20: Single-qubit Clifford commutation relations.

Chapter 3

Pauli Gadgets

Pauli gadgets are a class of unitary transformations that can be used to naturally represent the excitation operators used in UPS ansätze (Section 1.4). In this chapter, we introduce Pauli gadgets and their representation in the ZX calculus. We then develop a method for deriving a set of commutation relations that describes the interaction of Pauli gadgets with the Pauli and the Clifford gates. In Chapter 5, we use Pauli gadgets to construct one-body and two-body excitation operators before using the commutation relations derived here in a number of derivations.

A Pauli string P is defined as a tensor product of Pauli matrices $\{I, X, Y, Z\}^{\otimes n}$, where n is the number of qubits in the system, and each Pauli gate acts on a distinct qubit. Thus $Z \otimes X$ represents the Pauli Z and X gates acting on the first and second qubits respectively. *Stone's Theorem* [23] states that a strongly-continuous one parameter unitary group $U(\theta) = \exp\left(-i\frac{\theta}{2}H\right)$ is generated by the Hermitian operator H. Since Pauli strings are Hermitian, we can define Pauli gadgets as the one parameter unitary groups generated by the Pauli strings.

$$\Phi_1(\theta) = \exp\left(-i\frac{\theta}{2}Z \otimes I \otimes Z\right) \qquad \Phi_2(\theta) = \exp\left(-i\frac{\theta}{2}Y \otimes Z \otimes X\right)$$

Figure 3.1: Two examples of Pauli gadgets.

3.1 Phase Gadgets

Phase gadgets are defined as the one parameter unitary groups of Pauli strings consisting of only the Pauli I and Z matrices, $P \in \{I, Z\}^{\otimes n}$. They can be naively implemented as a Z rotation sandwiched between two ladders of CNOT gates.

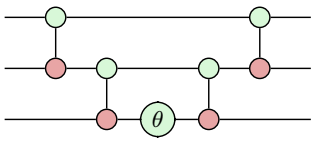

$$= \exp\left(-i\frac{\theta}{2} Z \otimes Z \otimes Z\right)$$

Phase gadgets correspond to unitary maps which are diagonal in the Z computational basis [10]. Consequently, they apply a global phase to a state without changing the distribution of the observed state [3]. Phase gadgets have the following representation in the ZX calculus.

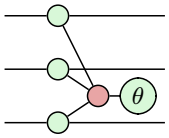

$$= \exp\left(-i\frac{\theta}{2} Z \otimes Z \otimes Z\right)$$

Phase gadgets can be interpreted as first copying each input in the Z basis (2.15), computing the parity of the state by taking the XOR (2.15), then multiplying the state by $\exp\left(-i\frac{\theta}{2}\right)$ or $\exp\left(i\frac{\theta}{2}\right)$ depending on the state's parity [3]. Using the identity (2.11), spider fusion (2.10) and bialgebra (2.16) rules, we are able to derive its representation in the ZX calculus.

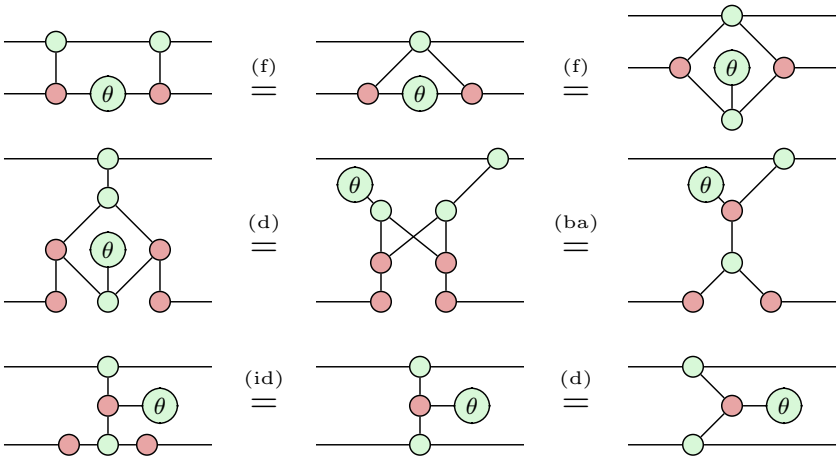

Figure 3.2: Phase gadget result.

It is then a simple matter of recursively applying this result to phase gadgets in quantum circuit notation to generalise to arbitrary arity.

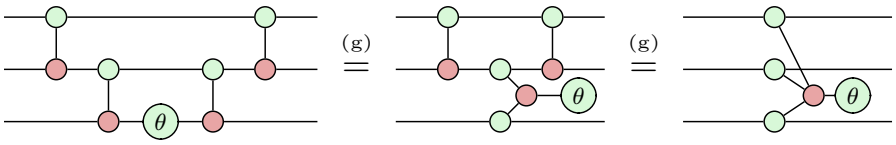

As well as being intuitively self-transpose, and hence diagonal, this representation comes equipped with various rules describing the interactions of phase gadgets.

Phase Gadget Identity

Phase gadgets with an angle $\theta = 0$ can be shown to be equivalent to identity using the state copy (2.12), spider fusion (2.10) and identity removal (2.11) rules.

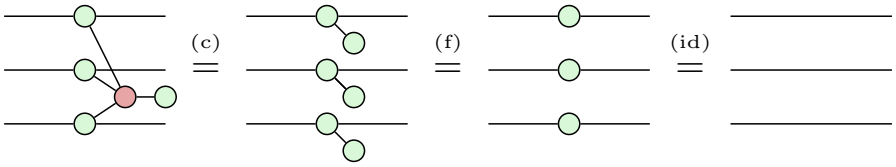

Phase Gadget Fusion

Using the spider fusion (2.10) and bialgebra (2.16) rules, we can show that phase gadgets with the same distribution of legs fuse together and their phases add.

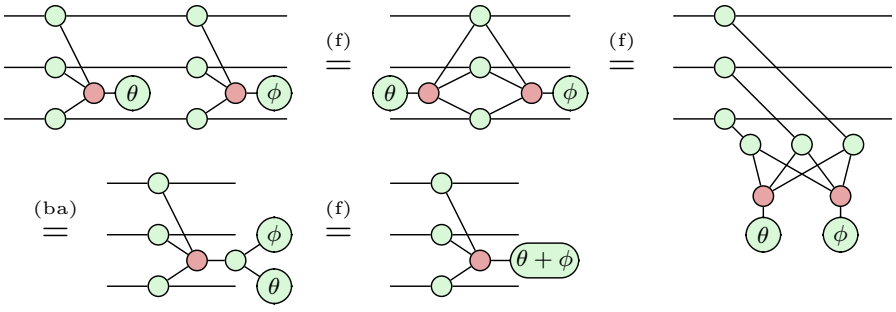

Phase Gadget Commutation

Phase gadgets can be shown to commute using the spider fusion rule (2.10).

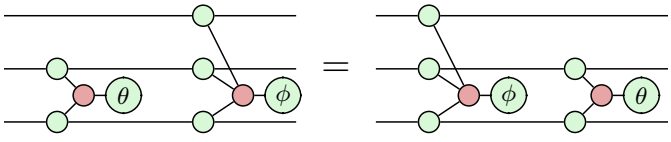

Phase Gadget Decomposition

Using the bialgebra rule (2.16), we can show that a two-legged phase gadget can be decomposed in the following two ways.

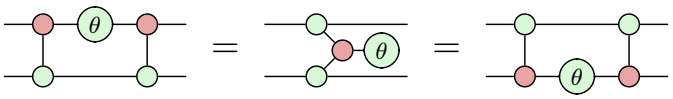

Figure 3.3: Phase gadget decomposition result.

By recursively applying this decomposition, we can show that it is possible to decompose a phase gadget in the balanced tree representation such that it has a circuit depth of $2\log_2(n)$, rather than $2(n-1)$ in the ladder representation [24], where n is the number of qubits.

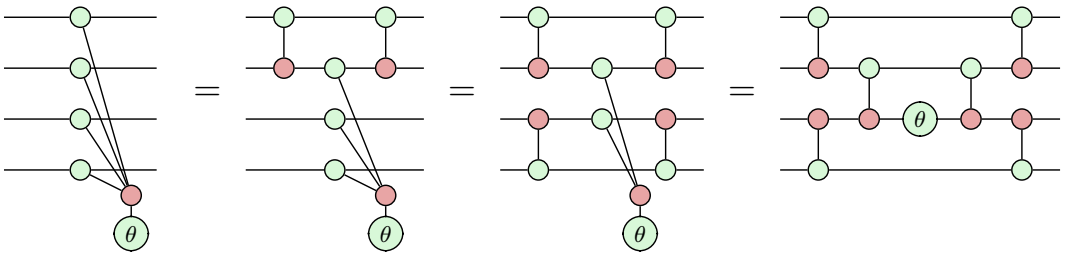

Figure 3.4: Balanced tree phase gadget decomposition.

Phase gadgets can be thought of as the many-qubit generalisation of a Z rotation (1.9). For instance, using the bialgebra (2.16), spider fusion (2.10), state copy (2.12) and identity (2.11) rules, we can demonstrate the correspondence between single-legged phase gadgets and Z rotations.

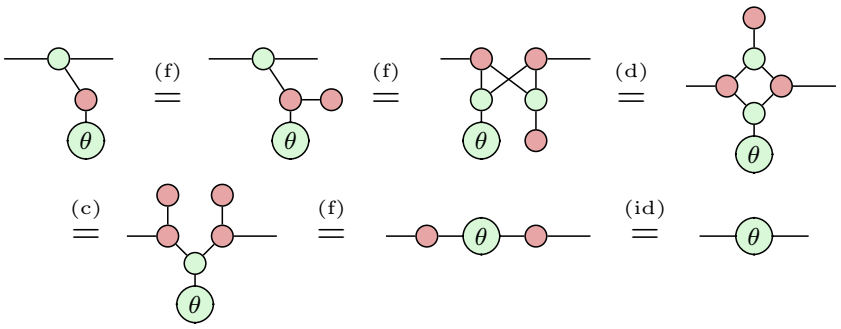

Figure 3.5: Single-legged phase gadget as a Z rotation.

3.2 Pauli Gadgets

Pauli gadgets are defined as the one parameter unitary groups of Pauli strings in the set $\{I, X, Y, Z\}^{\otimes n}$. By performing a Clifford conjugation (2.3) on the legs of a phase gadget, we obtain the corresponding Pauli gadget. That is, Pauli gadgets are phase gadgets associated with a change of basis. Hence, whilst phase gadgets alone cannot alter the distribution of the observed state, Pauli gadgets can [3].

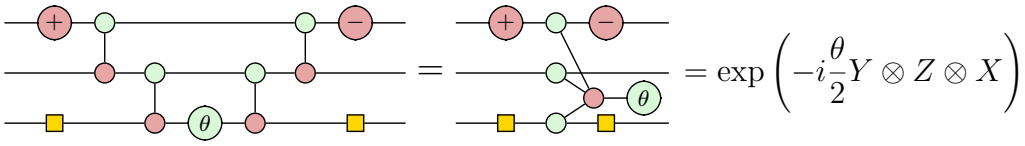

Pauli gadgets come equipped with a similar set of rules to phase gadgets that describe their interactions with other gadgets. For instance, adjacent Pauli gadgets with *matching legs* fuse, and their phases add modulo 2π.

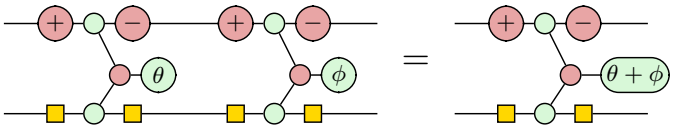

Figure 3.6: Pauli gadget fusion rule.

Similar to the phase gadget commutation rule (3.1), we have that adjacent Pauli gadgets with *no mismatching legs* commute.

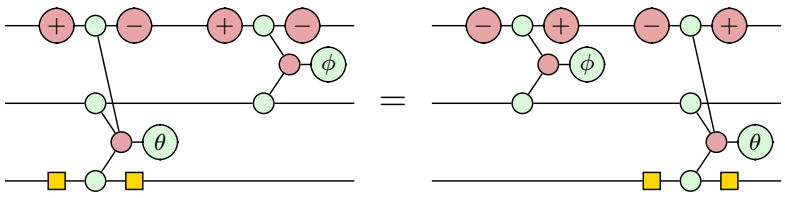

Figure 3.7: Pauli gadget commutation rule.

Single-legged Pauli gadgets correspond to rotations in their respective basis.

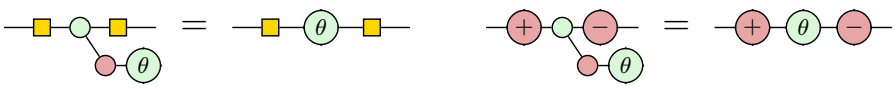

3.3 Phase Polynomials

Recalling that phase gadgets are diagonal in the computational Z basis, we refer to a set of Pauli gadgets as diagonal when it consists only of phase gadgets [10]. Such sets of phase gadgets are known as *phase polynomials* and are themselves diagonal in the computational Z basis [24]. Phase polynomial synthesis refers to finding a quantum circuit that optimally implements some phase polynomial, for which there are several well-known algorithms [25], [26], [27].

As in Cowtan *et al* [10], a set of Pauli gadgets S can be simultaneously diagonalised by a Clifford subcircuit C when all of the Pauli gadgets in the set commute. That is, by conjugating a set of commuting Pauli gadgets, we can re-express the circuit as some phase polynomial that can later be synthesised in some optimal way.

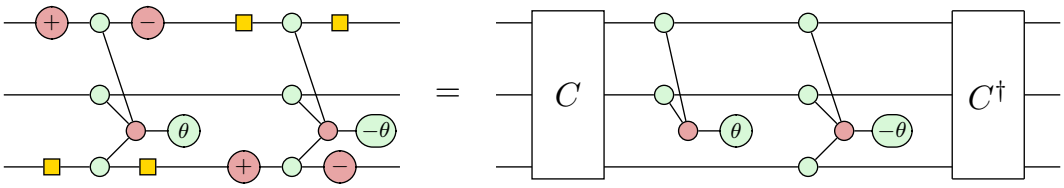

Figure 3.8: Diagonalisation of a pair of commuting Pauli gadgets by C.

As we will see in Chapter 5, the excitation operators used in VQE algoriths consist of commuting sets of Pauli gadgets. Therefore, the quantum circuits implementing such excitation operators can be diagonalised with some Clifford subcircuit C. As stated in Cowtan *et al* [10], whilst diagonalisation may incur gate overhead, in practice, the reduction in circuit depth arising from synthesising the resulting phase polynomial usually more than makes up for the overhead.

3.4 Commutation Relations

A pair of Pauli gadgets commute when their Hamiltonians commute. That is, a pair of Pauli gadgets commute when the Pauli strings that they are defined by also commute. Diagrammatically, we have that a pair of Pauli gadgets commute when they *mismatch on an even number of legs* [3]. Let us demonstrate this by first considering the three possible mismatching pairs of Pauli gadget legs.

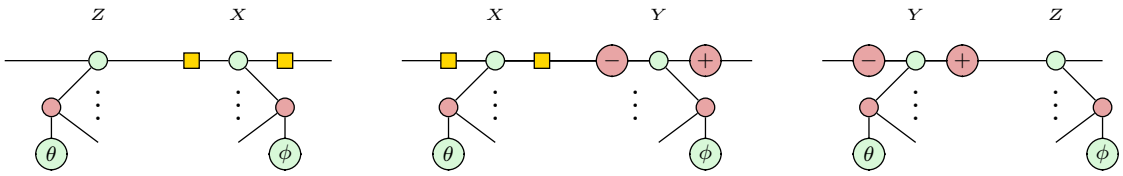

Starting with the mismatching Z/X pair and using the bialgebra (2.16), Hadamard commutation (2.14) and spider fusion (2.10) rules, we can show that commuting the gadgets' legs introduces a Hadamard between the bodies of the gadgets [3].

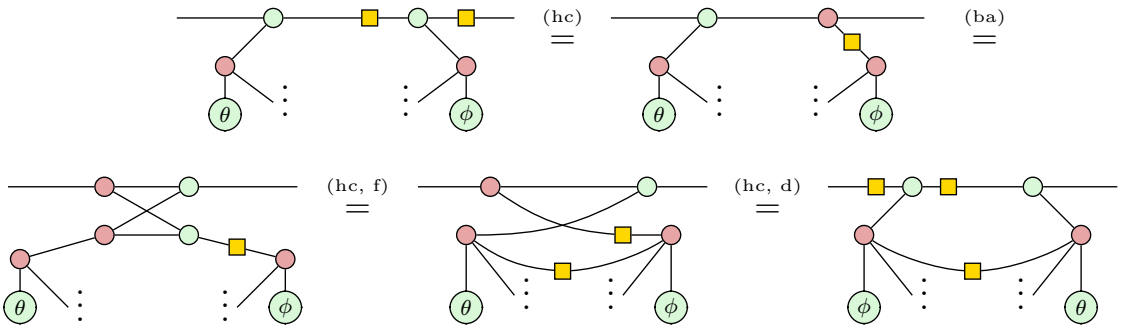

Similarly, for the X/Y and Y/Z mismatching pairs, we have the following.

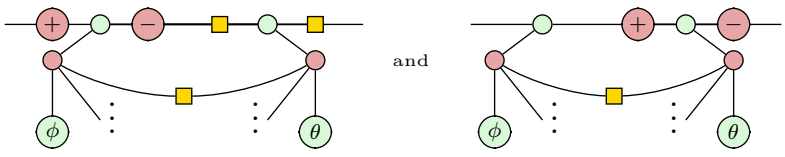

Therefore, we can show that two Pauli gadgets with an even number of mismatching legs commute by first commuting all of their legs, then using the Hopf rule (2.17) to remove the wires between them [3].

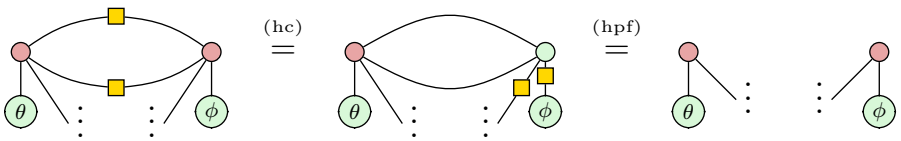

Clifford Commutation Relations

We now develop a set of *commutation relations* describing the interaction of Pauli gadgets with members of the Clifford group. Diagrammatically, we interpret this as 'what happens when a Clifford gate is pushed through a Pauli gadget'.

By definition, conjugating a Pauli string by a member of the Clifford group, $C^\dagger P C$, is closed in the set of Pauli strings, $\{I, X, Y, Z\}^{\otimes n}$, where n is the number of qubits that the Pauli string acts on. Similarly, conjugating a Pauli gadget $\Phi(\theta)$ by a member of the Clifford group always yields another Pauli gadget $\Phi'(\theta) = C^\dagger \Phi(\theta) C$.

Taking $C = \mathrm{CNOT}_{1,2}$, we can interpret the conjugation of a *phase gadget* diagrammatically (diagram on left) as the phase gadget decomposition result (3.3). Recalling that the members of the Clifford group are unitary transformations, $C^{-1} = C^\dagger$, we define *commutation relation* as $\Phi(\theta) C = C\, \Phi'(\theta)$ (diagram on right).

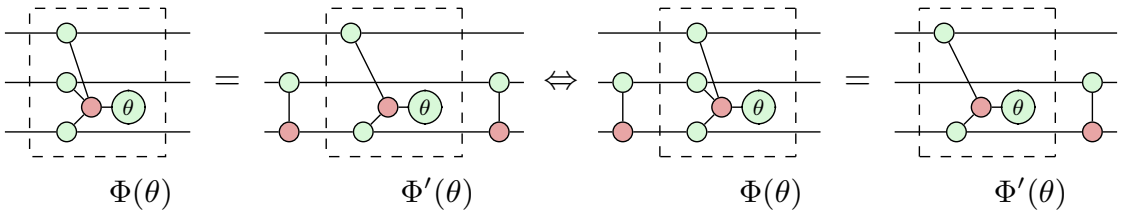

Since the CNOT and CZ gates act on two qubits ($n = 2$), we can form 16 unique Pauli gadgets from the set of Pauli strings $\{I, X, Y, Z\}^{\otimes 2}$. Consequently, we must derive 16 commutation relations to fully describe the interaction of Pauli gadgets with the CNOT and CZ gates.

Whilst it is possible to derive each of these commutation relations directly, it can be shown, through the relevant Taylor expansion, that conjugating a Pauli gadget is equivalent to finding the one parameter unitary group of the corresponding conjugated Pauli string. In other words, identifying how a Pauli string interacts with Clifford gates tells us how the corresponding Pauli gadget behaves.

Let us illustrate this with an example. Using the $Z \otimes Z$ Pauli string, we show that the $\mathrm{CNOT}_{0,1}$ gate commutes through the $\exp\left[-i\frac{\theta}{2}(Z \otimes Z)\right]$ gadget to give the $\exp\left[-i\frac{\theta}{2}(I \otimes Z)\right]$ gadget. We first push the bottom Pauli Z gate through the

CNOT target using the π copy rule (2.12), then, we push the top Pauli Z gate through the CNOT control using the spider fusion rule (2.10), cancelling one of the copied Pauli Z gates in the process.

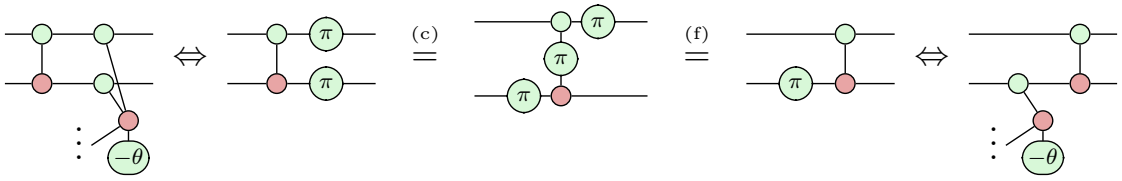

The Pauli Y gate is obtained by conjugating the Pauli Z gate with Clifford gates (2.18). Using the π copy (2.12) and spider fusion (2.10) rules, we can show that $Y = XZ$ up to a global phase of i and $Y = ZX$ up to a global phase of $-i$.

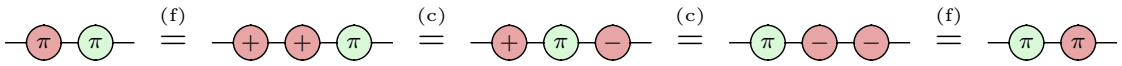

In the example below, one of the definitions of the Pauli Y gate above to derive how the CNOT gate interacts with the $\exp\left[-i\frac{\theta}{2}\left(Y \otimes X\right)\right]$ Pauli gadget by identifying how it gate interacts with the $Y \otimes X$ Pauli string.

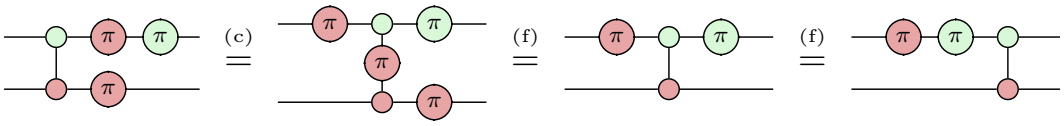

Similarly, we can identify how single-qubit gates interact with Pauli gadgets by identifying how they interact with the Pauli gates. In the example below, we use the fact that the above definitions of the Pauli Y gate differ by a factor of -1 to show that commuting a Hadamard through a Y leg flips the gadget's phase.

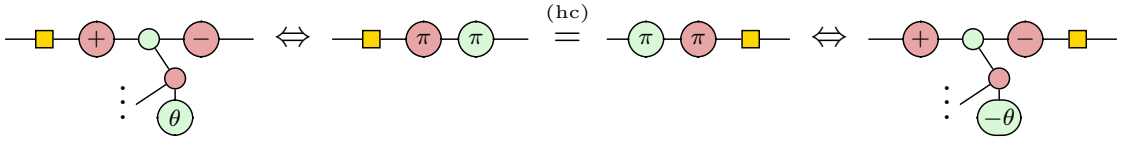

Using the rules described in this section, we were able to identify how Pauli gadgets interact with the Clifford and Pauli gates, in agreement with [3] and [24]. We have summarised these commutation relations below. In Chapter 5, we demonstrate how these commutation relations can be used to prove several important results.

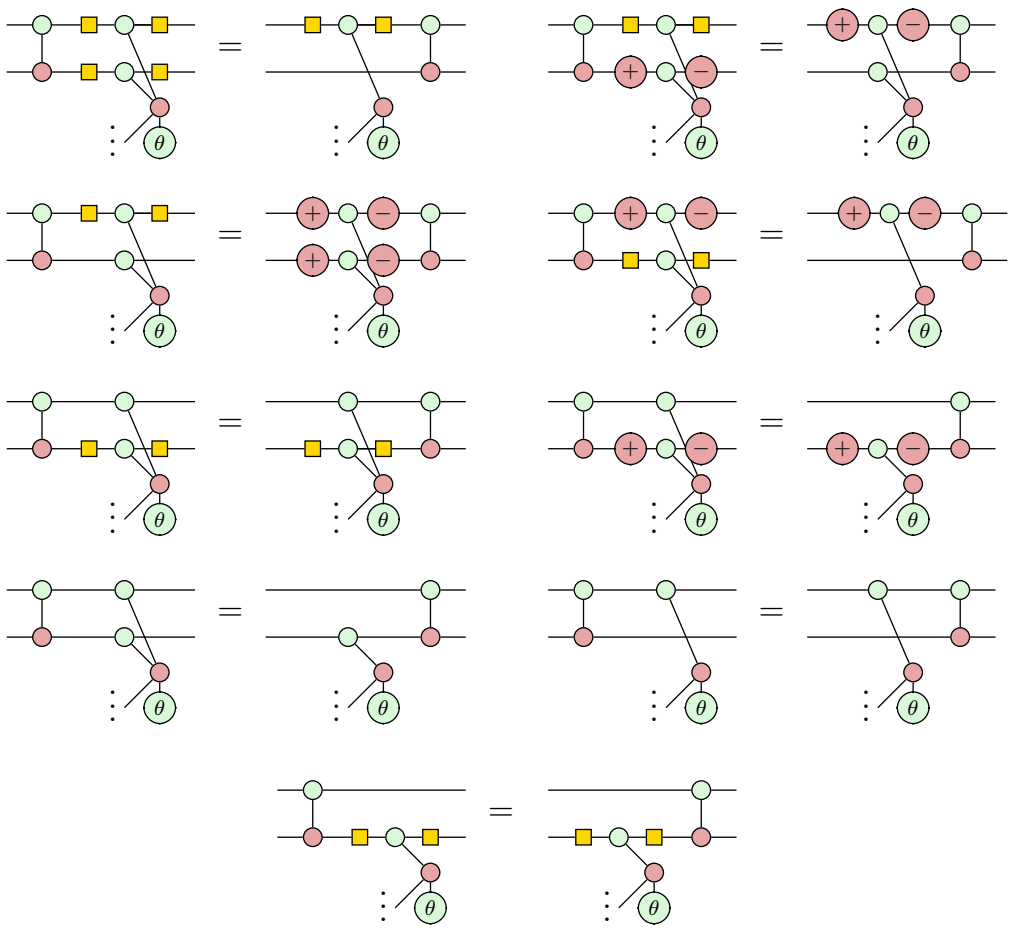

Figure 3.9: CNOT commutation relations excluding repetitions.

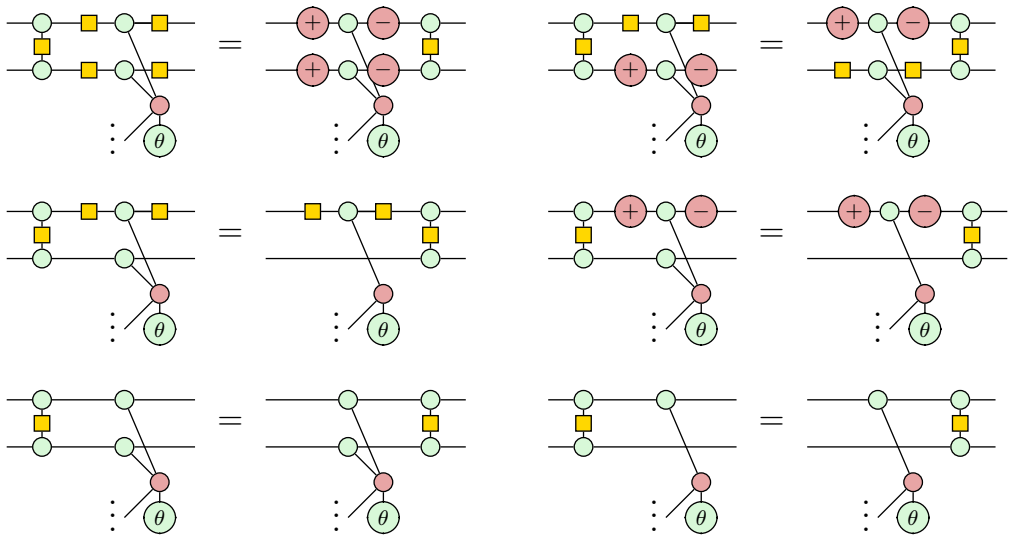

Figure 3.10: CZ commutation relations excluding repetitions.

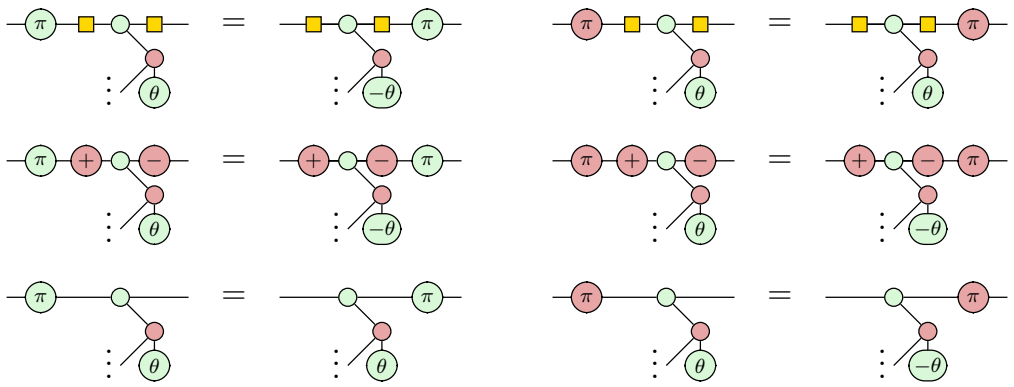

Figure 3.11: Pauli commutation relations.

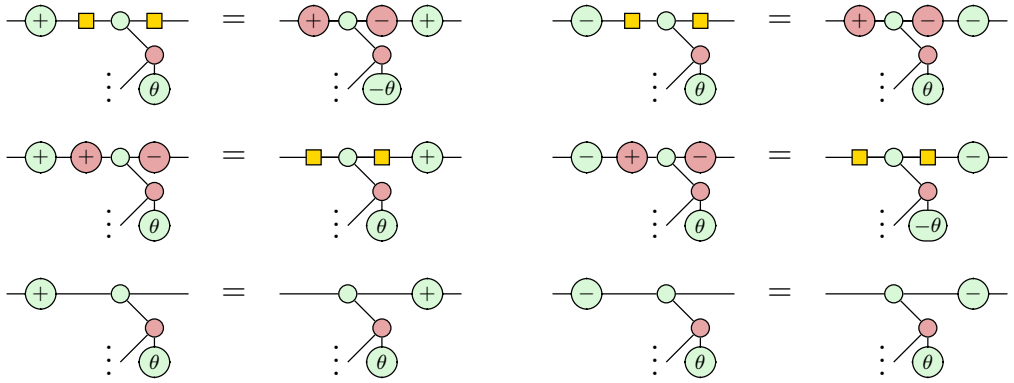

Figure 3.12: Clifford Z commutation relations.

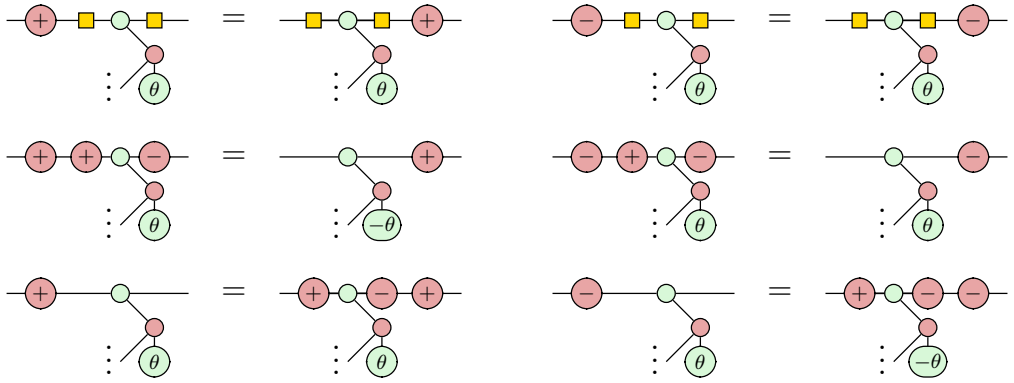

Figure 3.13: Clifford X commutation relations.

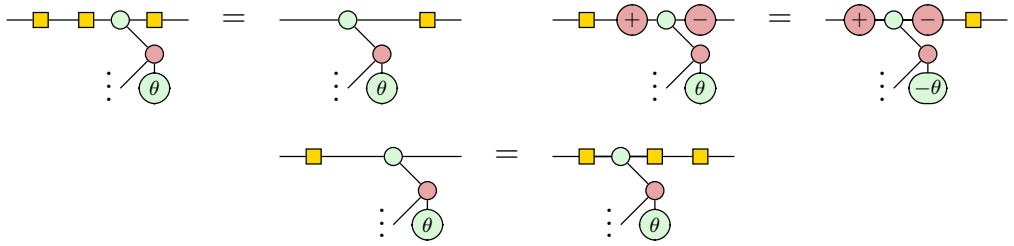

Figure 3.14: Hadamard commutation relations.

Chapter 4

Controlled Rotations

On our journey to identify a generalised representation for excitation operators in the ZX calculus, we came across the work done by Yordanov *et al*, which shows that excitation operators can be re-expressed in terms of controlled rotations by through conjugation by some subcircuit. Our interpretation of this result is that controlled rotations can be used to account for the Pauli antisymmetry of fermionic systems by conditionally applying a phase (rotation) depending on the parity of the state. In other words, the rotation is *controlled* by the parity of the state.

In this chapter, we begin by discussing the well-established representation of singly-controlled rotations the ZX calculus. We then demonstrate how these singly-controlled rotations can be used to construct higher-order controlled rotations, developing a representation for them in terms of phase polynomials. This approach was undertaken independently and the conclusions drawn in this section constitute a substantial portion of the research conducted in this thesis, requiring the use of the Clifford commutation relations developed in Section 3.4.

4.1 Singly Controlled-Rotations

Starting with the singly-controlled Z rotation gate $\mathrm{CR}_Z(\theta)$, we will see that it can be expressed as a combination of phase gadgets, since it corresponds to a diagonal matrix in the computational Z basis [3].

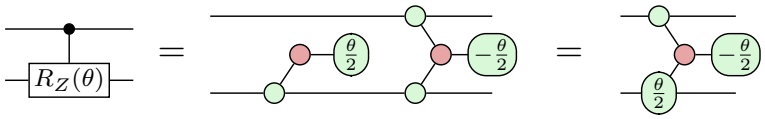

The $\mathrm{CR}_Z(\theta)$ gate applies a rotation to the target qubit if the control qubit is in the $|1\rangle$ state, and applies no rotation, if the control qubit is in the $|0\rangle$ state. This behaviour generalises to superpositions of states. Using the spider fusion (2.10) and bialgebra (2.16) rules, we obtain the following in quantum circuit notation.

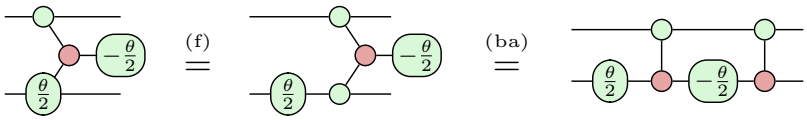

To verify that this circuit does indeed correspond to a controlled rotation in the Z basis, let us observe what happens when the control qubit is in the $|0\rangle$ state. Using the spider fusion (2.10), state copy (2.12) and identity (2.11) rules,

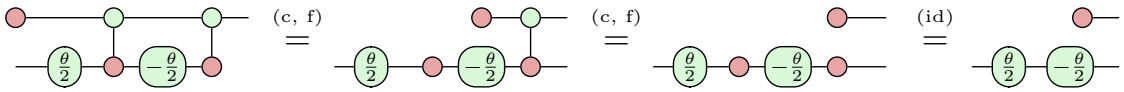

As expected, the resulting diagram fuses to give identity. Conversely, when the control qubit is in the $|1\rangle$ state, we obtain a Z rotation by θ.

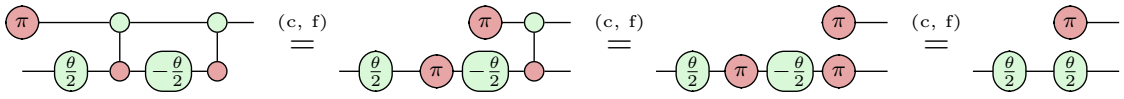

Using the the phase gadget fusion rule (3.1) and the phase gadget decomposition result (3.3), we can decompose the $\mathrm{CR}_Z(\theta)$ gate into four equivalent circuits.

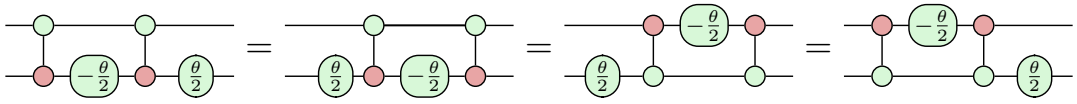

4.2 Higher Order Controlled-Rotations

We can implement higher order controlled rotations by nesting singly-controlled rotations as in Yordanov *et al* [9]. We implement a doubly-controlled Z rotation using two singly-controlled Z rotations with opposite phases as follows.

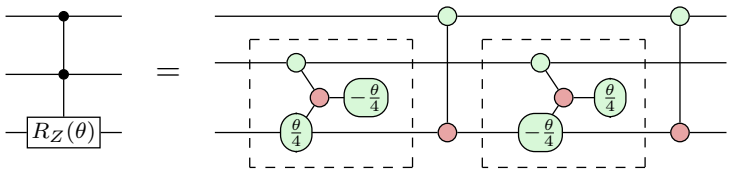

We can minimise the depth of the circuit implementing the $\mathrm{CCR}_Z(\theta)$ gate by choosing specific decompositions of the $\mathrm{CR}_Z(\theta)$ gate (left diagram) such that one pair of $\mathrm{CNOT}_{1,2}$ are adjacent and cancel one-another (right diagram).

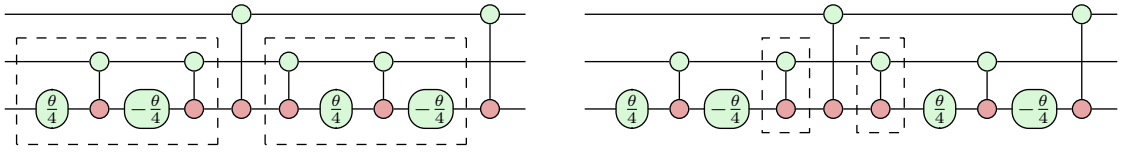

Figure 4.1: $\mathrm{CCR}_Z(\theta)$ circuit decomposition (left). Cancelling CNOT gate pair (right).

For the purposes of this thesis, we are interested in the form of controlled rotations in terms of Pauli gadgets. By expressing all Z rotations as phase gadgets (3.5) and commuting all CNOT gates through them such that the CNOT gates cancel, we obtain a phase polynomial consisting of four commuting phase gadgets.

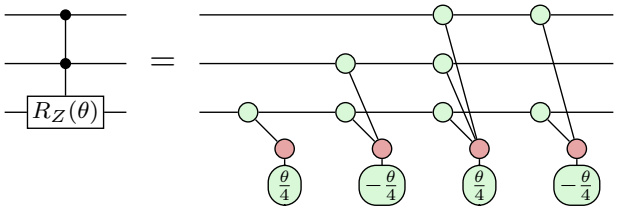

More generally, we can build controlled rotations of arbitrary arity by recursively nesting controled rotations as above. Hence, as with the doubly-controlled rotation, we can construct triply-controlled rotations by nesting two doubly-controlled rotations. Below is one specific circuit implementation of a triply-controlled Z rotation that maximises the number of cancelling CNOT gates.

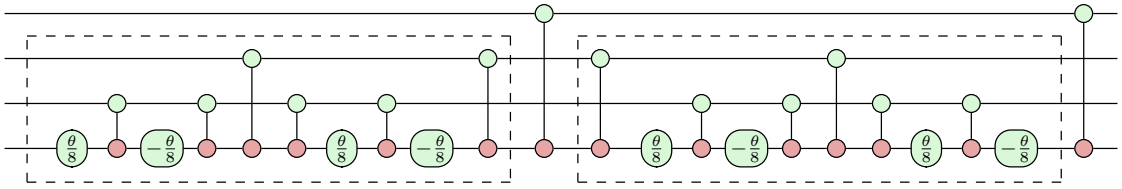

As before, we can show that the $\mathrm{CCCR}_Z(\theta)$ gate corresponds to a phase polynomial consisting of eight commuting phase gadgets.

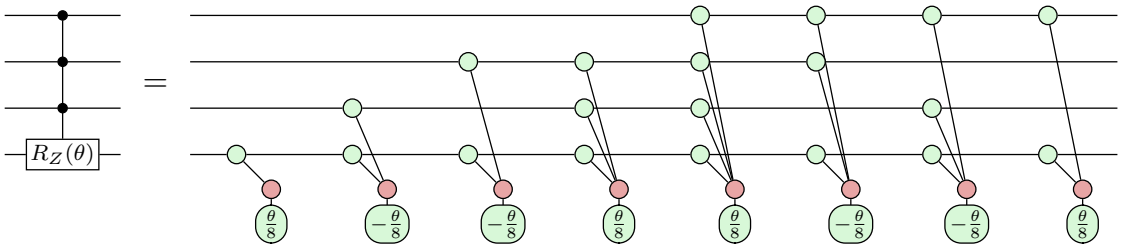

Controlled Rotations in Different Bases

By conjugating the target qubit with the correct Clifford gate (2.3), we obtain a controlled rotation in the desired basis. Consider the following examples.

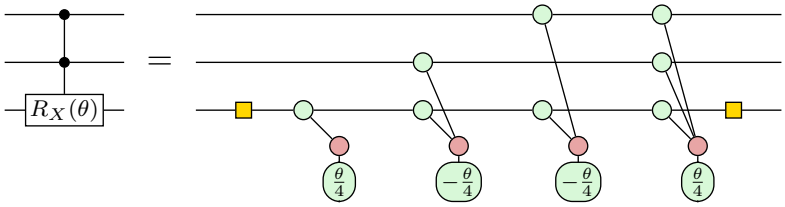

Figure 4.2: $\mathrm{CCR}_X(\theta)$ gate obtained by conjugating the $\mathrm{CCR}_Z(\theta)$ gate.

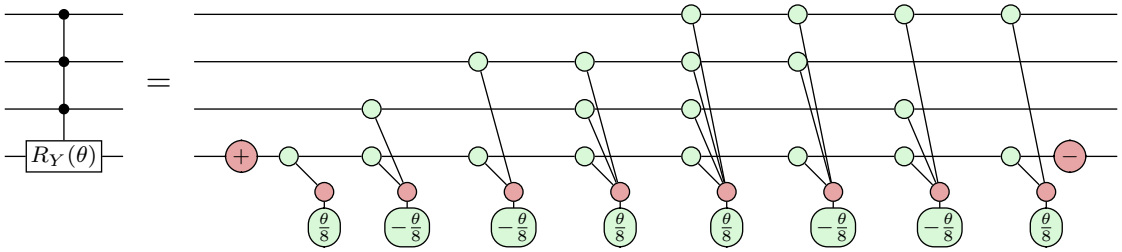

Figure 4.3: $\mathrm{CCCR}_Y(\theta)$ gate obtained by conjugating the $\mathrm{CCCR}_Z(\theta)$ gate.

Chapter 5

Excitation Operators

In this chapter, we discuss how the excitation operators used to construct UPS ansätze can be implemented on a quantum computer. We then use the ZX calculus to represent these excitation operators as Pauli gadgets and discuss ways in which we can optimise their circuits with respect to circuit depth. We then demonstrate how these excitation operators can be expressed in terms of controlled rotations (see Chapter 4) following conjugation by some subcircuit.

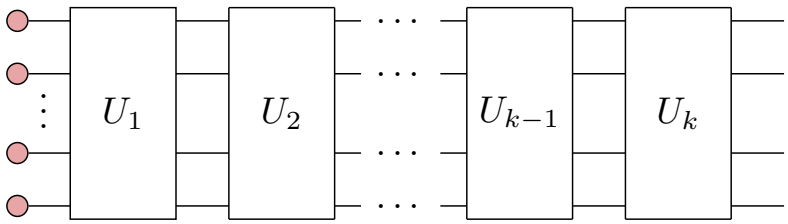

Figure 5.1: Example UPS ansatz approximating some fermionic ground state.

As stated in Cowtan *et al* [10], circuit optimisation amounts to pattern replacement, that is, recognising a subcircuit of a specific form and replacing it with an equivalent circuit that uses fewer quantum resources. Hence, by identifying the macroscopic structures representing these excitation operators, we facilitate the manipulation and optimisation of large-scale structures in the quantum circuit.

5.1 Implementing Excitation Operators

In Section 1.4, we showed that a fermionic state can be represented by a finite sequence of k parametrised one-body and two-body excitation operators acting on a single-Slater determinant reference state. After invoking the Trotter formula using one time step, we obtained the following equation for the UPS ansatz.

$$U(\boldsymbol{\theta}) = \prod_{m=1}^{k} U_m(\theta_m) \qquad U_m(\theta_m) = e^{\theta_m(\tau_m - \tau_m^\dagger)}$$

Figure 5.2: UPS ansatz (sequence of k one-body and two-body excitation operators).

In order to implement the fermionic excitation operators $U_m(\theta_m)$ on a quantum computer, we must first represent the second-quantised creation and annhilation operators in terms of quantum gates. For a single-state system, we do this by taking the following linear combinations of the Pauli gates.

$$\hat{a}^\dagger = |1\rangle\langle 0| = \frac{1}{2}(X - iY) \qquad \hat{a} = |0\rangle\langle 1| = \frac{1}{2}(X + iY)$$

Figure 5.3: Jordan-Wigner transformation for a single-state system.

Recalling that the creation and annhilation operators must preserve the fermionic anti-symmetry imposed by the Pauli principle, we modify these equations to account for the parity of the spin orbitals preceding the target spin orbital j when dealing with many-state systems. We do this by introducing a string of Pauli Z operators to compute the parity of the spin orbitals preceding spin orbital j.

$$\hat{a}_j^+ = \frac{1}{2}(X - iY)\bigotimes_{k=1}^{j-1} Z_k \qquad \hat{a}_j = \frac{1}{2}(X + iY)\bigotimes_{k=1}^{j-1} Z_k$$

Figure 5.4: Jordan-Wigner transformation for a many-state system.

This mapping is known as the Jordan-Wigner transformation [28] and has the advantage of preserving a direct mapping between fermionic states in the occupation

number representation and the qubit state vector. In other words, each qubit in our quantum circuit now encodes the occupation number of each spin orbital in our fermionic state $|f_{n-1} \dots f_0\rangle \ \rightarrow \ |q_{n-1} \dots q_0\rangle$.

Let us take the unitary operator $U_p^q(\theta)$ to be a one-body excitation operator derived from the anti-Hermitian second-quantised operator $a_q^\dagger a_p - a_p^\dagger a_q$ and acting on qubits p and q. After applying the Jordan-Wigner transformation to the second-quantised operator and exponentiating it, we obtain the following one-body excitation operator in terms of the Pauli matrices.

$$U_p^q(\theta) = \exp\left(i\frac{\theta}{2}(Y_pX_q - X_pY_q)\prod_{k=p+1}^{q-1} Z_k\right)$$

Figure 5.5: One-body excitaiton operator expressed in terms of the Pauli matrices.

By applying the Jordan-Wigner transformation to the two-body excitation operator $U_{pq}^{rs}(\theta)$, derived from the second-quantised operator $a_r^\dagger a_s^\dagger a_q a_p - a_p^\dagger a_q^\dagger a_s a_r$, we obtain the following two-body excitation operator in terms of the Pauli matrices.

$$U_{pq}^{rs}(\theta) = \exp\Bigg(i\frac{\theta}{8}(X_pX_qY_sX_r + Y_pX_qY_sY_r + X_pY_qY_sY_r + X_pX_qX_sY_r - Y_pX_qX_sX_r - X_pY_qX_sX_r - Y_pY_qY_sX_r - Y_pY_qX_sY_r)\prod_{k=p+1}^{q-1} Z_k \prod_{l=r+1}^{s-1} Z_l\Bigg)$$

Figure 5.6: Two-body excitation operator expressed in terms of the Pauli matrices.

Now that we have expressed the one-body and two-body excitation operators in terms of quantum gates, we discuss their specific implementations on a quantum computer. Starting with the one-body excitation operator, we can show that it can be expressed as the following product of commuting exponential terms.

$$U_p^q(\theta) = \left(\exp\left[i\frac{\theta}{2}Y_pX_q\prod_{k=p+1}^{q-1} Z_k\right]\right)\left(\exp\left[-i\frac{\theta}{2}X_pY_q\prod_{k=p+1}^{q-1} Z_k\right]\right)$$

Each exponential terms can be implemented by a quantum circuit consisting of a CNOT ladder construction conjugated by a Clifford subcircuit. By sequentially composing these circuits (2.1), that is taking their matrix product, we obtain the following quantum circuit.

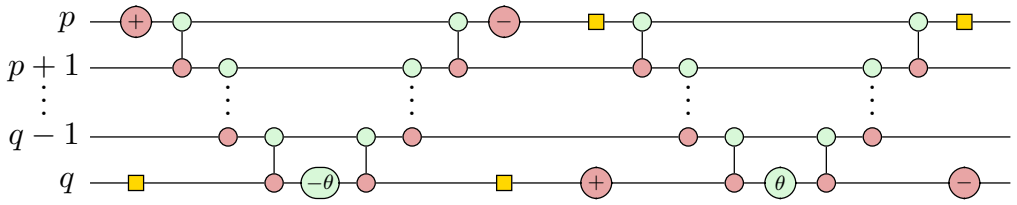

Figure 5.7: Circuit implementation of a one-body excitation operator.

The CNOT ladder constructions arise from exponentiating the string of Pauli Z gates, and serve to compute the parity of the spin orbitals between p and q, ensuring that the correct phase is applied to the fermionic state, and therefore accounting for the fermionic anti-symmetry imposed by the Pauli principle. The two-body excitation operator can similarly be factorised into eight commuting exponential terms, and is implemented by composing eight subcircuits.

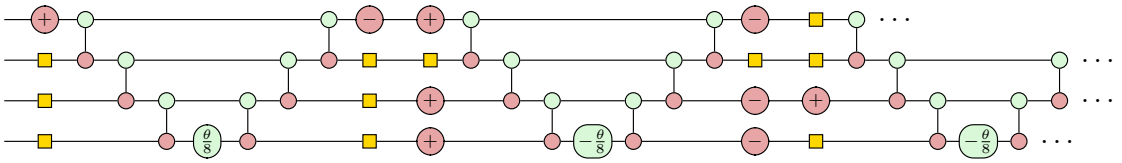

Figure 5.8: Circuit implementation of a two-body excitation operator.

Although essential for accurately simulating fermionic systems, these CNOT ladder constructions are extremely resource-intensive and contribute significantly to the circuit depth. The poor fidelity of today's quantum (NISQ) devices results in an accumulation of error as circuit depth increases. Consequently, we are interested in optimising these excitation operators with respect to circuit depth.

Excitation Operators as Pauli Gadgets

Using the phase gadget result (3.2) to collapse the CNOT ladder constructions, we can show that the quantum circuit implementing a one-body excitation operator

(Figure 5.7) corresponds to two commuting Pauli gadgets.

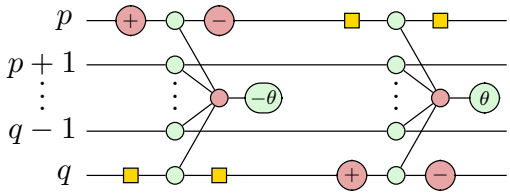

Similarly, we can show that the quantum circuit implementing a two-body excitation operator (Figure 5.8) corresponds to eight commuting Pauli gadgets.

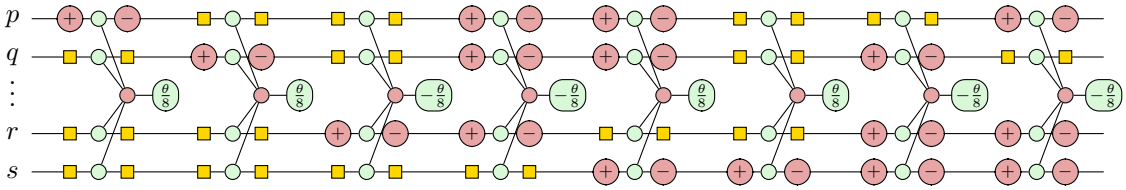

One immediate advantage of representing excitation operators in this form is that we can easily show that these Pauli gadgets do indeed commute by recognising that they have two mismatching pairs of legs (see Section 3.4). Another is that we can resynthesise the quantum circuit using the balanced tree decomposition result (3.4), yielding a circuit depth of $2\log_2(n)$ rather than $2(n-1)$.

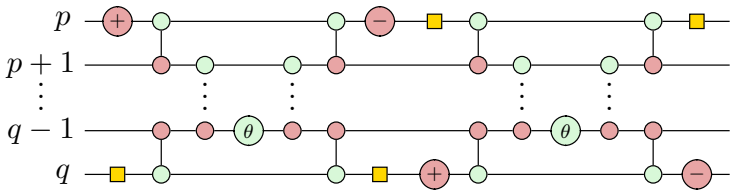

Figure 5.9: Balanced tree decomposition of a one-body excitation operator.

5.2 Commuting Excitation Operators

The DISCO-VQE algorithm generates multiple UPS ansätze, each yielding the same energy expectation value, but corresponding to a unique sequence of excitation operators. The identical energy expectation values of these UPS ansätze implies that they equivalently capture the correlation present in the molecular system of interest, suggesting that it may be possible to demonstrate an equivalence between them through algebraic manipulation. Motivated by this result, in this section we use the commutation rules developed in Section 3.4 to identify which excitation operators in the DISCO-VQE operator pool commute, and which do not.

We define *trivially commuting* excitation operators as commuting operators that act on a disjoint set of qubits, and *non-trivially commuting* excitation operators as commuting operators which act on an intersecting set of qubits. By expressing the excitation operators in the DISCO-VQE operator pool in terms of Pauli gadgets, we were able to identify several previously unknown non-trivially commuting pairs of excitation operators. We hope that by using these commutation relations, we might be able to demonstrate an equivalence between the UPS ansätze generated by the DISCO-VQE algorithm. Whilst we did not have sufficient time to attempt this, we leave it to future researchers to attempt. In the following graph, A – F represent one-body excitation operators and G – L represent two-body excitation operators. We have then drawn lines between commuting pairs.

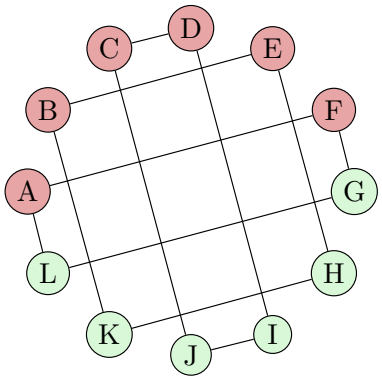

Figure 5.10: Graph identifying commuting operators used in the DISCO-VQE algorithm.

5.3 Excitations as Controlled Rotations

In this chapter, we replicate the results of Yordanov and Kornell in the ZX calculus using the representation of higher-order controlled rotations developed in Chapter 4, as well as the commutation relations derived in Chapter 3.4.

We began this research with the goal of identifying a generalised structure for the excitation operators used in the DISCO-VQE algorithm, in the ZX calculus. This led us to the work done by Yordanov *et al* [9] and Kornell *et al* [29], which demonstrate that it is possible to reveal an underlying controlled rotation within each excitation operator by conjugating it with some subcircuit.

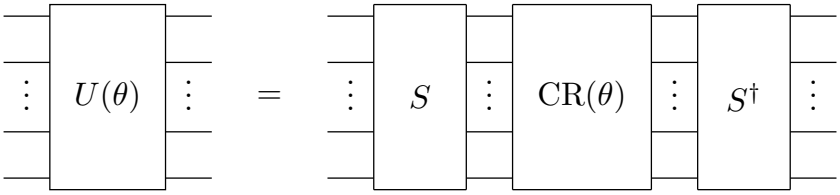

Figure 5.11: Conjugating $U(\theta)$ by subcircuit S to reveal a controlled rotation $\mathrm{CR}(\theta)$.

One-body excitation operators (5.7) and two-body excitation operators (5.8) have large circuit depths as a result of the multiple CNOT ladder constructions used to compute the parity of the fermionic state. Yordanov *et al* suggest that by rewriting the excitation operators in terms of controlled rotations, we can significantly reduce the circuit depth. We begin by demonstrating this result using a minimal one-body excitation operator, implemented by the following quantum circuit.

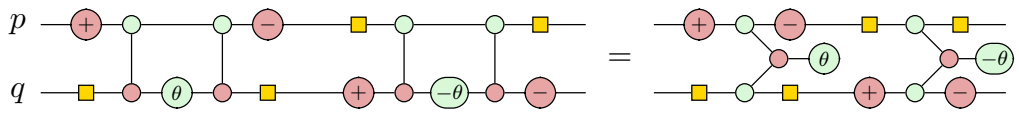

Figure 5.12: Quantum circuit (left) and in Pauli gadget form (right).

By inserting two adjacent (self-inverse) $\mathrm{CNOT}_{0,1}$ gates into the circuit and using the CNOT commutation relations (3.9) derived in Chapter 3, we can show that the one-body excitation operator above corresponds to a singly-controlled Y rotation.

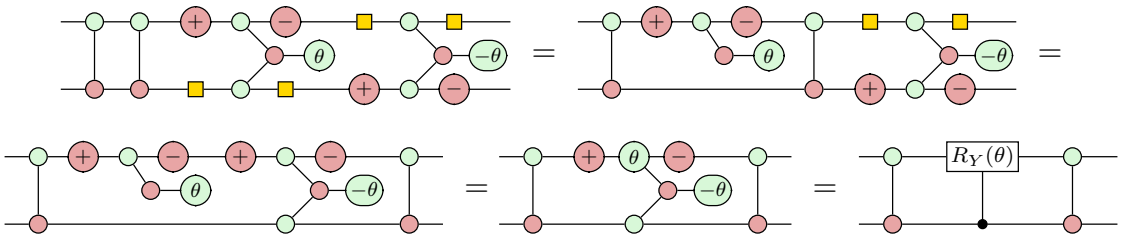

Had we instead chosen to insert two $\mathrm{CNOT}_{1,0}$ gates, we would have obtained the following controlled rotation, with the first qubit being the control.

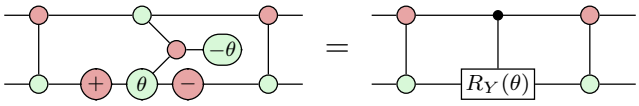

Let us now look at the general one-body excitation operator. We begin by conjugating with CNOT gates and a CZ gate (2.9) using the CNOT commutation relations (3.9) and CZ commutation relations (3.10) derived in Section 3.4.

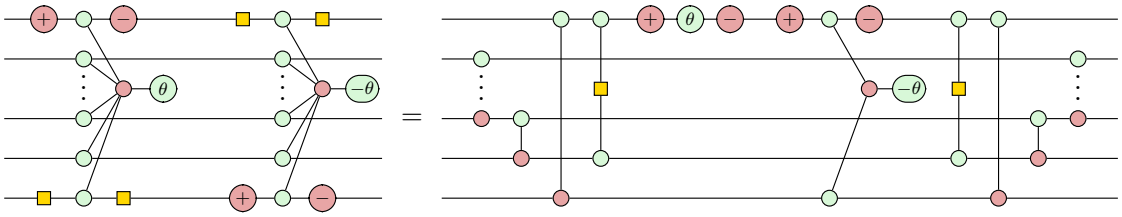

Then, by fusing the single-qubit Y rotation with the adjacent Pauli gadget, we reveal a singly-controlled Y rotation, as discussed in Chapter 4. In this way, we have succesfully replicated the result in Yordanov *et al* [9] using the ZX calculus.

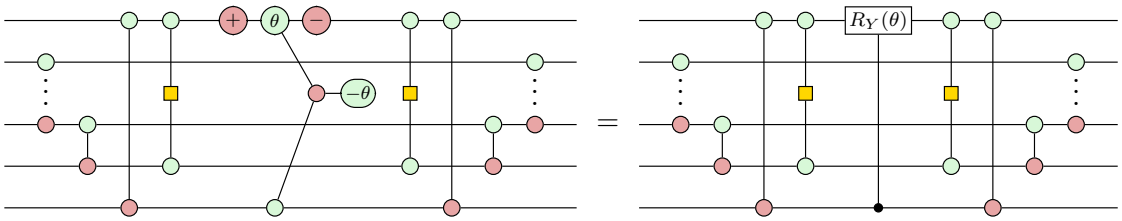

Let us now consider the two-body excitation operator, represented as follows.

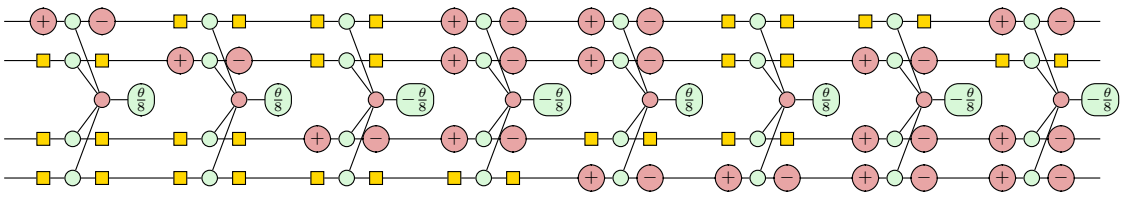

We begin by conjugating the circuit with three CNOT gates using the CNOT commutation relations (3.9) derived in Section 3.4.

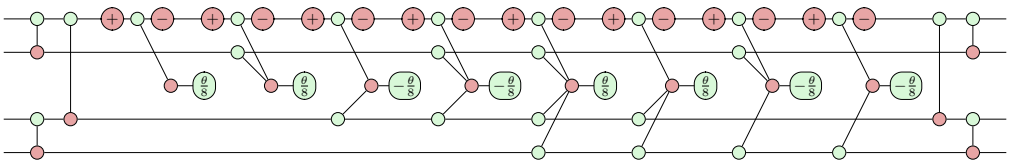

Then, by cancelling the adjacent Clifford gates, we reveal a phase polynomial.

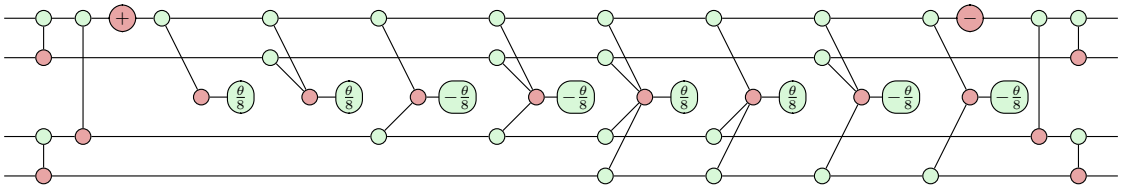

Finally, by conjugating the circuit with Pauli X gates on the second and fourth qubits, using the Pauli X commutation relations (3.11), we flip the phases of some of the phase gadgets, ensuring that the phase polynomial matches the result for the triply-controlled Y rotation in Figure 4.3. Note that the *first qubit* corresponds to the target, and the *second, third and fourth qubits*, correspond to the controls.

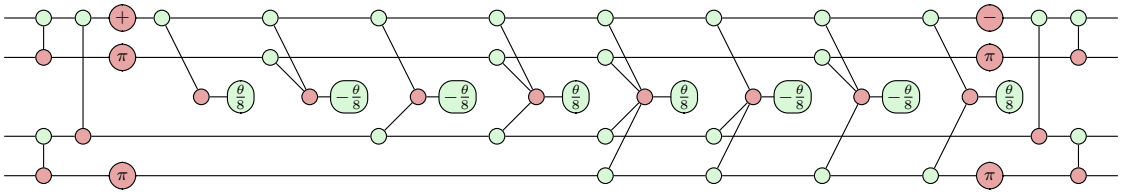

The target qubit is conjugated by Cliffords, putting it in the Y basis, and since the controls on the second and fourth qubits are conjugated by Pauli X gates, they must be in the $|0\rangle$ (rather than $|1\rangle$) state, to activate the rotation. We have, therefore, succesfully replicated the result in Yordanov *et al* [9] using the ZX calculus.

At the expense of introducing additional quantum gates, we have eliminated the resource-intensive CNOT ladder constructions associated with the two subcircuits in the one-body excitation operator and the eight subcircuits in the two-body excitation operator. By choosing efficient implementations of controlled Y rotations, we can then offset the gate overhead introduced by the additional quantum gates.

Similarly, Kornell *et al* [29] show that by conjugaing the two-body excitation operator with the following subcircuit, we obtain the same triply-controlled Y rotation. We were able to demonstrate this in the ZX calculus as follows.

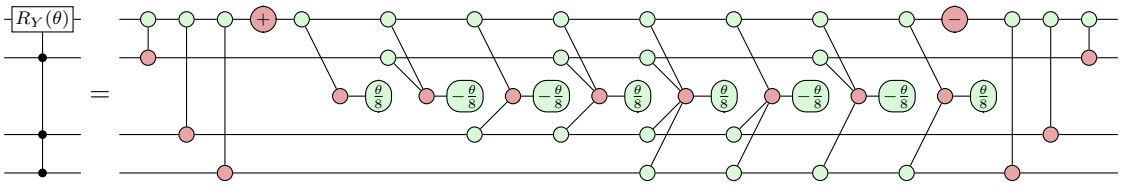

In Chapter 6, we introduce a software package called ZxFermion that we developed to facilitate this type of derivation. Using ZxFermion, we were able to identify that it is possible to choose the control and target qubits of the triply-controlled rotation by conjugating with the following subcircuits.

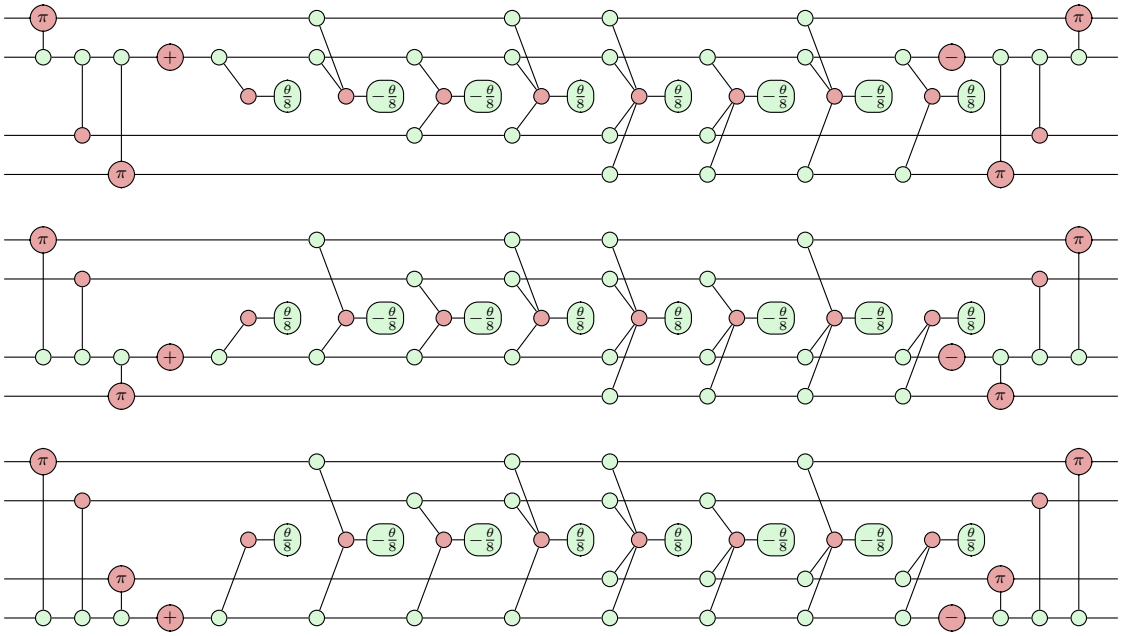

Chapter 6

ZxFermion Software

Visit **github.com/aymannel/zxfermion** for complete documentation.

Motivated by the need for an accessible tool to explore research ideas related to circuits of Pauli gadgets, we decided to build the ZxFermion Python package for the visualisation and manipulation of circuits of Pauli gadgets. It is built on top of the PyZX `BaseGraph` API [30] and the Stim `Tableau` class [31].

ZxFermion provides classes to represent Pauli gadgets and common quantum gates and encodes the commutation relations developed in Section 3.4. It is designed to integrate within Jupyter notebook environments, enabling users to generate interactive ZX diagrams directly in the output cell. ZxFermion offers an accessible tool for studying the interactions of Pauli gadgets in the context of VQE.

Using ZxFermion, we can replicate all of the commutation relations described in Section 3.4 as well as the proofs discussed in Chapter 5, showcasing a noteworthy acceleration in research pace. We anticipate that both chemists and computer scientists exploring quantum computing within the VQE framework will find this software tool advantageous.

Remark – *The ZxFermion package has undergone thorough testing, ensuring its reliability and ease of use.*

6.1 Creating Gadgets and Circuits

We begin by introducing the `Gadget` class, which we use to represent Pauli gadgets. The `Gadget` class takes a Pauli string and a phase as inputs. For instance, we instantiate the exp $\left[-i\frac{1}{4}\left(Y\otimes Z\otimes X\right)\right]$ gadget as follows.

```
gadget = Gadget('YZX', phase=1/2)
gadget.draw()
```

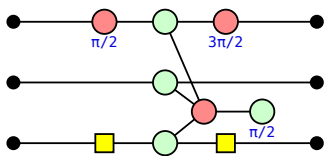

By setting `as_gadget=False`, we expand the gadget in quantum circuit notation.

```
gadget = Gadget('YZX', phase=1/2, as_gadget=False)
gadget.draw()
```

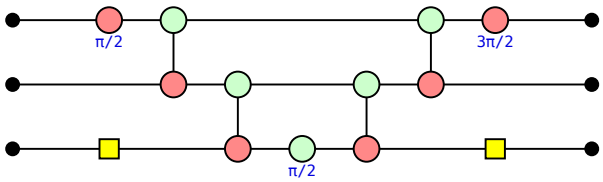

We can construct a circuit of Pauli gadgets using the `GadgetCircuit` class, providing it with an ordered list of `Gadget()` objects. For instance, we implement a one-body excitation operator below, as discussed in Chapter 5.

```
gadget1 = Gadget('YZX', phase=1/2)
gadget2 = Gadget('XZY', phase=3/2)
circuit = GadgetCircuit([gadget1, gadget2])
circuit.draw()
```

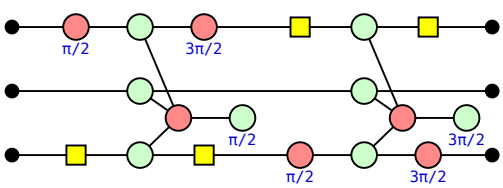

We now introduce the classes implementing the standard quantum gates. As we will see in Section 6.2, ZxFermion encodes the logic describing the interaction of

the these gates with Pauli gadgets, allowing us to replicate the results in Chapter 5. The CNOT and CZ gates are implemented by the `CX` and `CZ` classes respectively. We can specify the control and target qubits using the `control` and `target` parameters. When not specified, these parameters default to `control=0` and `target=1`.

```
gates = [CX(), CZ(1, 2), CX(0, 2), CZ(0, 1)]
circuit = GadgetCircuit(gates)
circuit.draw()
```

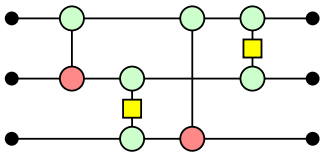

The Pauli Z and Pauli X gates are implemented by the `Z` and `X` classes respectively. We specify the target qubit using the `qubit` parameter (defaults to `qubit=0`).

```
gates = [X(), Z(0), X(0), Z(1), X(1), Z(1)]
circuit = GadgetCircuit(gates)
circuit.draw(stack=True)
```

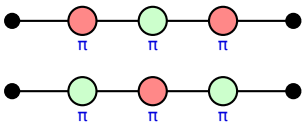

Similarly, the single-qubit Clifford gates are implemented by the `ZPlus`, `ZMinus`, `XPlus` and `XMinus` classes. Below we implement the $Y \otimes Y$ Pauli string (Section 2.3).

```
gates = [XPlus(), Z(0), XMinus(0), ZMinus(1), X(1), ZPlus(1)]
circuit = GadgetCircuit(gates)
circuit.draw(stack=True)
```

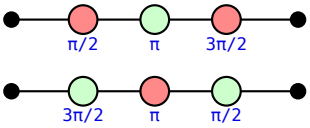

Finally, we have the Hadamard gate, which is implemented by the `H` class.

```
circuit = GadgetCircuit([H()])
circuit.draw()
```

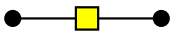

6.2 Manipulating Circuits

The `GadgetCircuit` class offers the ability to manipulate circuits containing Pauli gadgets via the `apply()` method. This method takes a quantum gate object as its input and inserts it, along with its adjoint, into the circuit. The `start` and `end` parameters allow us to specify the insertion positions.

```
gadget = Gadget('YZ', phase=1/2)
circuit = GadgetCircuit([gadget])
circuit.apply(CX(0, 1), start=0, end=0, draw=True)
```

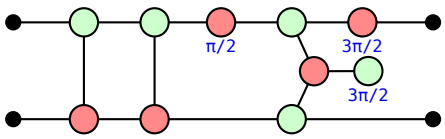

If no insertion positions are specified, the specified quantum gate and its adjoint are inserted at the start and at the end of the circuit respectively. The relevant commutation relations developed in Section 3.4 are then applied as required.

```
gadget = Gadget('YZ', phase=1/2)
circuit = GadgetCircuit([gadget])
circuit.apply(CX(0, 1), draw=True)
```

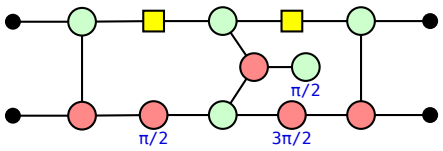

The `apply()` method is not limited to CNOT gates – we could have instead chosen any of the quantum gates mentioned in the previous section. The commutation logic uses Stim's `Tableau` class to construct the required Clifford tableau ensuring that the correct transformation is applied. Below we conjugate with the CZ gate.

```
gadget = Gadget('XY', phase=1/2)
circuit = GadgetCircuit([gadget])
circuit.apply(CZ(0, 1), draw=True)
```

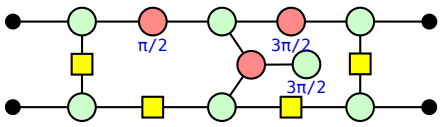

The `GadgetCircuit` class offers the ability to manipulate circuits containing multiple gadgets simultaneously. Below, we instantiate the minimal one-body excitation operator discussed in Figure 5.12.

```
gadget1 = Gadget('YX', phase=1/2)
gadget2 = Gadget('XY', phase=3/2)
circuit = GadgetCircuit([gadget1, gadget2])
circuit.draw()
```

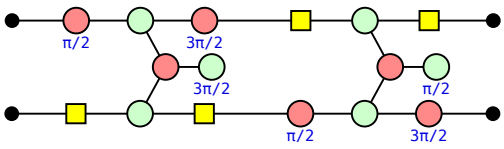

It is then simply a matter of conjugating with CNOT gates to replicate the derivation revealing a singly-controlled Y rotation, as shown in Section 5.3.

```
circuit.apply(CX(0, 1), draw=True)
```

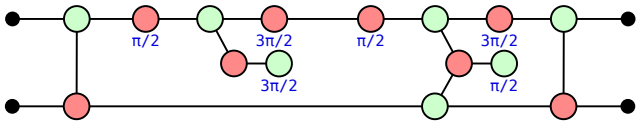

We can replicate the derivation that reveals a singly-controlled Y rotation from a one-body excitation operator shown in Section 5.3. We begin by instantiating the `GadgetCircuit()` object with the following lines of code.

```
gadgets = [Gadget('YZZZX', phase=1/2), Gadget('XZZZY', phase=-1/2)]
circuit = GadgetCircuit(gadgets)
circuit.draw(as_gadgets=True)
```

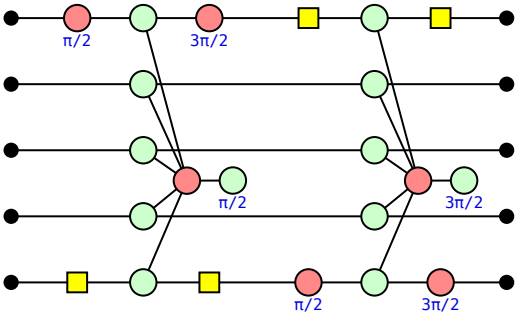

Then, using the following lines of code, we eliminate the Z legs responsible for calculating the parity of the fermionic state, and reveal the two Pauli gadgets, that

together, correspond to a singly-controlled Y rotation.

```
circuit.apply(CX(1, 2), start=0, end=2)
circuit.apply(CX(2, 3), start=1, end=-1)
circuit.apply(CZ(3, 0), start=2, end=-2)
circuit.apply(CX(0, 4), start=3, end=-3)
circuit.draw()
```

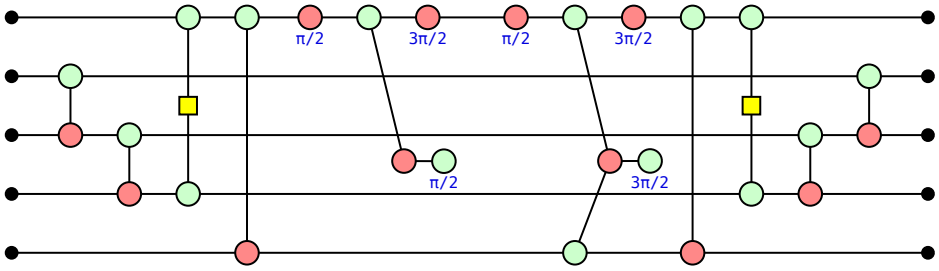

Similarly, we can replicate the derivation in Kornell *et al* [29]. We begin by instantiating the `GadgetCircuit()` object as follows.

```
gadgets = [
    Gadget('YXXX', phase=1/8),  Gadget('XYXX', phase=1/8),
    Gadget('XXYX', phase=-1/8), Gadget('YYYX', phase=-1/8),
    Gadget('YYXY', phase=1/8),  Gadget('XXXY', phase=1/8),
    Gadget('XYYY', phase=-1/8), Gadget('YXYY', phase=-1/8)
]

circuit = GadgetCircuit(gadgets)
circuit.draw()
```

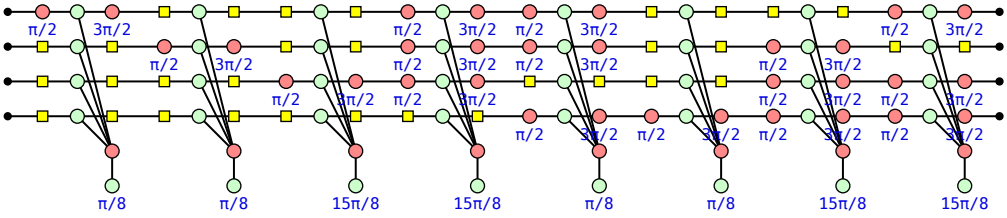

Then, using the following lines of code, we reveal a triply-controlled Y rotation.

```
circuit.apply(CX(0, 3), draw=False)
circuit.apply(CX(0, 2), draw=False)
circuit.apply(CX(0, 1), draw=True)
```

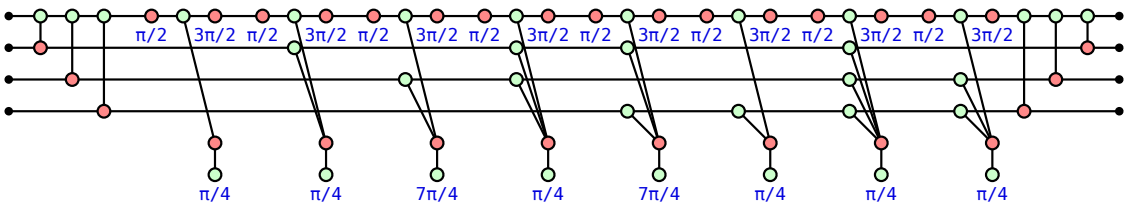

Chapter 7

Conclusion

7.1 Summary

7.2 Future Work

- diagonalise commuting pairs of operators

Bibliography

[1] Szalay, P. G., Müller, T., Gidofalvi, G., Lischka, H. & Shepard, R. Multiconfiguration self-consistent field and multireference configuration interaction methods and applications. *Chemical Reviews* **112**, 108–181 (2011).

[2] Kassal, I., Whitfield, J. D., Perdomo-Ortiz, A., Yung, M.-H. & Aspuru-Guzik, A. Simulating chemistry using quantum computers. *Annual Review of Physical Chemistry* **62**, 185–207 (2011).

[3] Yeung, R. Diagrammatic design and study of ansätze for quantum machine learning (2020). 2011.11073.

[4] Preskill, J. Quantum computing in the nisq era and beyond. *Quantum* **2**, 79 (2018).

[5] Burton, H. G. A., Marti-Dafcik, D., Tew, D. P. & Wales, D. J. Exact electronic states with shallow quantum circuits from global optimisation. *npj Quantum Information* **9** (2023).

[6] Wecker, D., Hastings, M. B. & Troyer, M. Progress towards practical quantum variational algorithms. *Physical Review A* **92**, 042303 (2015).

[7] McClean, J. R., Romero, J., Babbush, R. & Aspuru-Guzik, A. The theory of variational hybrid quantum-classical algorithms. *New Journal of Physics* **18**, 023023 (2016).

[8] Kirby, W. M. & Love, P. J. Variational quantum eigensolvers for sparse hamiltonians. *Phys. Rev. Lett. 127, 110503 (2021)* **127**, 110503 (2020). 2012.07171.

[9] Yordanov, Y. S., Arvidsson-Shukur, D. R. M. & Barnes, C. H. W. Efficient quantum circuits for quantum computational chemistry. *Physical Review A* **102**, 062612 (2020).

[10] Cowtan, A., Simmons, W. & Duncan, R. A generic compilation strategy for the unitary coupled cluster ansatz (2020). 2007.10515.

[11] Coecke, B. & Duncan, R. Interacting quantum observables: categorical algebra and diagrammatics. *New Journal of Physics* **13**, 043016 (2011).

[12] Cerezo, M. *et al.* Variational quantum algorithms. *Nature Reviews Physics 3, 625-644 (2021)* **3**, 625–644 (2020). 2012.09265.

[13] Szabó, A. v. & Ostlund, N. S. *Modern quantum chemistry : introduction to advanced electronic structure theory* (Mineola (N.Y.) : Dover publications, 1996). URL http://lib.ugent.be/catalog/rug01:000906565.

[14] Helgaker, T., Jørgensen, P. & Olsen, J. *Molecular Electronic-Structure Theory* (Wiley, 2000).

[15] Fetter, A. L., Walecka, J. D. & Kadanoff, L. P. *Quantum Theory of Many Particle Systems*, vol. 25 (AIP Publishing, 1972).

[16] Nielsen, M. A. & Chuang, I. L. *Quantum Computation and Quantum Information: 10th Anniversary Edition* (Cambridge University Press, 2012).

[17] Taube, A. G. & Bartlett, R. J. New perspectives on unitary coupled-cluster theory. *International Journal of Quantum Chemistry* **106**, 3393–3401 (2006).

[18] Peruzzo, A. *et al.* A variational eigenvalue solver on a photonic quantum processor. *Nature Communications* **5** (2014).

[19] Evangelista, F. A., Chan, G. K.-L. & Scuseria, G. E. Exact parameterization of fermionic wave functions via unitary coupled cluster theory. *The Journal of Chemical Physics* **151** (2019). 1910.10130.

[20] Poór, B. *et al.* Completeness for arbitrary finite dimensions of zxw-calculus, a unifying calculus (2023). 2302.12135.

[21] van de Wetering, J. Zx-calculus for the working quantum computer scientist (2020). 2012.13966.

[22] Grier, D. & Schaeffer, L. The classification of clifford gates over qubits. *Quantum 6, 734 (2022)* **6**, 734 (2016). 1603.03999.

[23] Stone, M. H. On one-parameter unitary groups in hilbert space. *The Annals of Mathematics* **33**, 643 (1932).

[24] Cowtan, A., Dilkes, S., Duncan, R., Simmons, W. & Sivarajah, S. Phase gadget synthesis for shallow circuits (2019). 1906.01734.

[25] Amy, M., Maslov, D., Mosca, M. & Roetteler, M. A meet-in-the-middle algorithm for fast synthesis of depth-optimal quantum circuits. *IEEE Transactions on Computer-Aided Design of Integrated Circuits and Systems* **32**, 818–830 (2013).

[26] Amy, M., Maslov, D. & Mosca, M. Polynomial-time t-depth optimization of clifford+t circuits via matroid partitioning. *IEEE Transactions on Computer-Aided Design of Integrated Circuits and Systems* **33**, 1476–1489 (2014).

[27] Nam, Y., Ross, N. J., Su, Y., Childs, A. M. & Maslov, D. Automated optimization of large quantum circuits with continuous parameters. *npj Quantum Information* **4** (2018).

[28] Seeley, J. T., Richard, M. J. & Love, P. J. The bravyi-kitaev transformation for quantum computation of electronic structure. *The Journal of Chemical Physics* **137** (2012). 1208.5986.

[29] Kornell, A. & Selinger, P. Some improvements to product formula circuits for hamiltonian simulation (2023). 2310.12256.

[30] Kissinger, A. & van de Wetering, J. Pyzx: Large scale automated diagrammatic reasoning. *Electronic Proceedings in Theoretical Computer Science* **318**, 229–241 (2020).

[31] Gidney, C. Stim: a fast stabilizer circuit simulator. *Quantum* **5**, 497 (2021).